University of Alabama in Huntsville
LOUIS

Theses | UAH Electronic Theses and Dissertations

2024

A novel dual-band outline elliptical dipole antenna for passive energy harvesting

Jonathan Marquardt

Follow this and additional works at: https://louis.uah.edu/uah-theses

Recommended Citation
Marquardt, Jonathan, "A novel dual-band outline elliptical dipole antenna for passive energy harvesting" (2024). *Theses*. 677.
https://louis.uah.edu/uah-theses/677

This Thesis is brought to you for free and open access by the UAH Electronic Theses and Dissertations at LOUIS. It has been accepted for inclusion in Theses by an authorized administrator of LOUIS.

A NOVEL DUAL-BAND OUTLINE ELLIPTICAL DIPOLE ANTENNA FOR PASSIVE ENERGY HARVESTING

by

Jonathan Marquardt

A THESIS

Submitted in partial fulfillment of the requirements
for the degree of Master of Science
in
The Department of Electrical and Computer Engineering
to
The Graduate School
of
The University of Alabama in Huntsville

HUNTSVILLE, ALABAMA
2021

Approved by:
Dr. Maria Pour, Committee Chair
Dr. Laurie Joiner, Committee Member
Dr. Tony Gatlin, Committe Member
Dr. Aleksandar Milenković, Department Chair
Dr. Shankar Mahalingam, College Dean
Dr. Jon Hakkila, Graduate Dean

ABSTRACT
The School of Graduate Studies
The University of Alabama in Huntsville

Degree: Master of Science in Engineering

College/Dept.: Electrical and Computer Engineering

Name of Candidate: Jonathan Marquardt

Title: A Novel Dual-Band Outline Elliptical Dipole Antenna for Passive Energy Harvesting

In this thesis, a new dual-band antenna is presented for use in space-based passive energy harvesting. This antenna is based on elliptical dipole antennas, which are often used for their ultra-wideband (UWB) properties. The inner metallization is removed, leaving an outline antenna and room for a second set of antenna arms. This will in turn result in an interleaved structure to tune each set of dipole arms to two different frequencies. Due to the close proximity of the dipole arms there exists strong mutual coupling, which is lessened by adding decoupling elements to the design.

The proposed antenna is supported by a partial ground plane to improve the front-to-back ratio of the radiation patterns. Different design iterations are full-wave analyzed in which the ground plane is extended with an exponential taper and additional parasitic elements are added to improve antenna performance. Sweeps are then carried out to show the effects of the eccentricity of the outer ellipse and the effects of the curvature of the extended ground plane. An additional method of reducing the board size is presented as well. Finally, the dual-band elliptical outline design was fabricated and

measured and the results found to be in good agreement with simulation. This antenna design provides good impedance matching, peak gain, and radiation pattern for both of the bands of interest.

ACKNOWLEDGMENTS

I would like express my deepest thanks to my advisor, Dr. Maria Pour, for all of her help and patience in guiding me through the difficult processes of conducting research and writing my thesis. I would also like to thank Curtis Hill and all of the staff at the Marshall Space Flight Center that I have met and worked with for providing feedback and suggestions throughout the course of this project. I am grateful to my colleague Saininad Naik for providing instruction in a few difficult technical challenges. I would also like to express my gratitude to my committee members, Dr. Laurie Joiner and Dr. Tony Gatlin. Finally, I'd like to thank all of my friends and loved ones for providing support to me during my time as a graduate student.

This work was supported in part by NASA's Marshall Space Flight Center in Huntsville, AL, under a cooperative agreement award.

Table of Contents

List of Figures

LIST OF TABLES

CHAPTER 1

Introduction

1.1 Preface

The use of antennas for powering remote circuitry has its roots in the earliest days of experimental electromagnetism. Heinrich Hertz demonstrated a high-frequency, highly-directed system for transmitting and receiving power based on parabolic dishes [1]. The need for extremely narrow beamwidths for efficient active power transmission, however, has persisted as an obstacle to the use of antennas to power devices. Some use of wireless power transfer has been seen for orbital satellites, including the use of an antenna array and a rectifier driven by a transmitted signal from the Space Shuttle [2]. An alternative approach for low-power applications is passive energy harvesting, in which an antenna and a rectifier are used without an active source transmitting power via a directive antenna. Instead, ambient electromagnetic energy is recycled to drive low-power components.

For a NASA space-based application, an antenna is desired that could receive ambient energy at two separate frequency bands of 0.915 GHz and 2.45 GHz. This antenna is to have at least 10 dB return loss, 10 dB front-to-back ratio, and positive peak gain in the forward direction, preferably greater than 3 dBi. Additionally, this antenna

should be compact, low-profile, and lightweight.

1.2 Research Objective

The objective of this thesis is to present a design for a dual-band antenna suitable for space-based energy harvesting. We do this with the following:

- Investigate the single-band elliptical antenna and study the effect of removing the interior metallization using a full-wave electromagnetic solver.
- Use this interior space to insert a second set of antenna arms to operate at a higher frequency band for dual-band operation.
- Apply a series of design alterations to improve impedance matching, forward gain, and front-to-back ratio in both bands to acceptable levels.
- Prototype and measure the dual-band design to validate our simulated antenna models.

1.3 Thesis Overview

A brief overview of the thesis structure is as follows:

Chapter 1 gives an introduction of the topics of elliptical dipole antennas, dual-band antennas, and passive energy harvesting. It provides objectives for the thesis and gives an outline of the contents. Chapter 2 reviews the state-of-the-art technologies that relate to this thesis and provides a brief background theory on the antenna design topics covered. Chapter 3 details the design procedure of the dual-band elliptical dipole by presenting the design evolution starting with the single-band filled elliptical dipole antenna. Several iterations on this design are presented in succession and the performance

improvements that motivate these alterations are detailed. Finally, the completed dual-band elliptical dipole antenna design proposed by this thesis is presented and the simulated performance discussed. In Chapter 4, several case studies are presented. First, a parametric sweep of the semi-major axis of the outer elliptical antenna arm is carried out, giving insight into how the antenna performance varies with the eccentricity of that shape. Second, a parameter controlling the shape of the ground plane backing the antenna is varied to determine the sensitivity of the antenna's performance to the ground plane. Lastly, the size of the board is further reduced and another design variation is proposed to compensate for the difficulties introduced by this reduction. Chapter 5 details the manufactured antenna prototype and compares the measured results with the simulated ones. Chapter 6 gives a summary of the thesis and discusses further avenues of study for this project.

CHAPTER 2

Literature Review and Theory

2.1 Introduction

For space-based antenna applications, size, weight, cost, and complexity are crucial considerations. A low-profile antenna is thus desired; double-sided printed antennas are an attractive option. These antennas simply consist of a printed circuit board (PCB) with radiating elements, such as the two arms of a dipole, etched or printed in conductor on either side of a dielectric. These antenna elements can be arranged into arrays for larger aperture size and increased gain, and so long as the thickness of the PCB is small compared to the wavelength at which the antenna operates it will behave similarly to a planar design [3]. This is useful as planar dipoles generate omnidirectional type radiation patterns, which are valuable to increase the power received by the antenna [4]. These double-sided printed dipole elements have promising potential to be used in larger arrays due to their low-cost, low-profile, wideband properties [5]. If additional bandwidth is desired, each arm of the dipole element can be replaced with an elliptical patch [6].

2.2 Bow-tie and Elliptical Antennas

To maximize the amount of ambient energy received, expanding the operation of the antenna and rectifier to operate over a larger bandwidth is a useful strategy [7]. Broadband antennas such as the biconical and spherical antennas and their two-dimensional counterparts, the bow-tie and circular antennas, have been characterized extensively in antenna literature [8]. Elliptic monopole antennas are well-studied as their eccentricity gives them greater bandwidth than a circular radiating element [9][10]. The bandwidth of elliptical antennas also exceeds that of other shapes such as square, rectangular, or hexagonal [11].

The bow-tie antenna is an appealing candidate for wideband applications due to its good impedance matching and flat gain response [12]. Rounding the edges of a bow-tie antenna confers some advantages; investigation of "rounded bow-tie" antenna designs shows a larger impedance bandwidth compared to the unaltered bow-tie [13][14]. Planar elliptical dipoles have also been studied for their ultra-wideband (UWB) capabilities, some giving more than two octaves of bandwidth with omnidirectional type radiation patterns [15]. These antennas can be quite compact, providing 10 dB of return loss with a minor axis of 0.2λ, where λ is the wavelength of the center frequency [15]. Increasing the axial ratio of the elliptical elements to 1.75 serves to improve the return loss characteristics without degrading the antenna radiation pattern along the major axis of the ellipses [15]. Planar elliptical dipoles have been shown to provide gain comparable to that of a linear dipole antenna but with superior bandwidth and impedance matching [16][17]. These planar dipoles have also been approximated by stepped polygons of

equivalent area to provide comparable performance [18].

In both the bow-tie and elliptical dipole designs, the literature suggests that it is not necessary to fill the full area occupied by the dipole arms with a conductor to achieve good impedance matching and efficient radiation. This is in part due to the fact that the surface current density is considerably higher at the edges of the bow-tie arms than at the centers, as reported in [19]. Here Durgun *et al.* investigated the effects of removing the center metallization from each arm to create an outline bow-tie antenna [19]. Their results show that removing the center metallization lowers the resonant frequency by 3.3% and contributes to a 0.8 dB decrease in gain, but otherwise the fractional impedance bandwidth and radiation pattern remained relatively unchanged [19]. The reduced frequency is expected as the antenna is now considerably miniaturized. Interestingly enough, removing the copper conductor inside of these arms also serves to reduce the weight of the antenna. Similarly, applying a circular slot within an elliptical patch does not significantly degrade the radiation pattern or impedance matching [20][21] [22]. If sufficient metallization is removed, the antenna begins to resemble a loop antenna. While at eccentricities close to zero (nearly circular) this elliptical loop behaves like a circular loop antenna, at higher eccentricities the elliptical loop behaves more similarly to a dipole [23]. Planar elliptical dipoles with elliptical slots have been studied for UWB applications and found to have increased gain and impedance bandwidth [24] [25][26].

2.3 Dual-band Antennas

An alternative to achieving good impedance matching and radiation

properties over an ultra-wide band is to target multiple, specific bands in which the aforementioned features are maintained. Many low-profile, compact designs for dual-band and multiband antennas have been proposed; often these are familiar antenna designs with features added to increase the current path and modify the surface current distributions of a designated mode, such as in the slotted microstrip patch antenna proposed by Maci *et al.* [27]. The double-sided printed dipole has also seen modification to create a dual-band sleeve dipole antenna [28]. A dual-band double-T monopole antenna has been constructed with a partial ground plane; it was found that the dimensions of this ground plane were critical in the operation of the antenna at the lower-band [29]. Double-sided printed bow-tie antennas have been modified for dual-band use by adding parasitic triangular elements in the space between the bow-tie arms [30].

Some multi-band antennas have been studied in which the inner metallization of an antenna element is removed and the resulting empty space filled with additional, smaller elements. These smaller elements are tuned to radiate at the higher frequencies of interest. This procedure has been applied to the double-sided rectangular dipole antenna, creating nested "frame" dipoles, for dual-band and triple-band operation [31]. Using multiple of these frame dipoles allows for independent tuning of the resonant frequencies of the antenna; each of these frame dipoles has a resonant frequency slightly below that of its filled dipole counterpart [31]. Finally, Song *et al.* have investigated the effects of nesting circular and elliptical ring monopole antennas within each other to excite multiple bands [32].

2.4 Slotted Ground Plane

One alteration that can be applied to antennas to suppress back radiation and improve impedance matching is the addition of quarter-wave chokes to the ground plane. This is part of a broader category of defected ground structure (DGS) techniques that have been studied in antenna literature to lessen the effects of edge diffraction on the ground plane [33]. This slotted DGS has been used to improve impedance matching and allow for multiband radiation for a circular disk antenna [34]. The effects of lateral and peripheral quarter-wave chokes, added to the conducting ground plane of a microstrip patch antenna as a primary feed in symmetric parabolic reflectors, on the cross polarization and back radiation were studied in [35]. It was shown that the peripheral chokes were most effective in reducing the back radiation regardless of the antenna size. It was later reported in [36] that adding four quarter-wave slots to the corners of the supporting ground plane for a microstrip patch resulted in less backward radiation [36].

2.5 Summary

The literature review presented in this chapter establishes the basis for the elements of our antenna design. The concept of powering devices via a power-harvesting antenna is introduced along with the benefits of using passive energy harvesting. The double-sided dipole family of antennas is appropriate for space-based passive energy harvesting applications due to their low-profile, lightweight topology. Elliptical antennas, including double-sided elliptical dipoles, have seen widespread use as UWB radiators along with their cousin the bow-tie antenna. Both bow-tie and elliptical antennas can still

function as efficient radiators with much of their interior metallization removed, albeit at the expense of bandwidth. This hollowed-out interior space can then be used for placing additional antenna elements for multiband operation. Finally, adding quarter-wave choke slots to a backing ground plane and forming a DGS can reduce the back radiation.

CHAPTER 3

Design Evolution from Single- to Dual-Band Printed Elliptical Antennas

3.1 Introduction

Here a novel dual-band antenna is proposed and its design procedure is detailed. This antenna is designed for use by the National Aeronautics and Space Administration (NASA) for space-based passive energy harvesting. It is to operate in a lower-band centered around 0.915 GHz and an upper-band at 2.45 GHz. The proposed design is low-profile, compact, and low-cost, and provides good performance in the areas of return loss, impedance bandwidth, peak gain, and front-to-back ratio in each band.

Early in the antenna's development, we explored a dual-band slotted microstrip patch antenna similar to the design proposed by Maci, *et al.* [27], by exciting the first two broadside transverse magnetic (TM) modes of a rectangular patch antenna, namely the TM_{10} and TM_{30} modes. Using slots parallel to the radiating edges of the patch allowed us to tune the resonant frequency of the TM_{30} mode to the upper band and create a broadside radiation pattern with suppressed sidelobes in the E-plane. Their proposed technique was for a range of frequency ratios from 1.6 to 2, and the frequency ratio could

be controlled by moving the slots inward on the patch. However, for our higher frequency ratio of 2.7, realizing enough bandwidth at each band, matching the input impedance, and achieving satisfactory sidelobe suppression seemed quite far-fetched using this method, especially on a very thin dielectric substrate. As such, we moved on to a dual-band elliptical antenna design, which is an excellent candidate for low-profile applications. Starting with a single-band, double-sided filled elliptical dipole antenna, we move towards the dual-band design presented at the end of the chapter.

3.2 Single-band Antennas

3.2.1 Filled Elliptical Dipole

To begin our investigation of this design, we will start with the double-sided elliptical dipole antenna. First, we will look at the "filled" antenna. This antenna, shown in Fig. 3.1, consists of two elliptical arms on either side of a dielectric substrate. The substrate is a 0.11 mm-thick Rogers Kappa 438 [37] with a dielectric constant of 4.38 and a loss tangent of 0.005. The ratio of major to minor axis was chosen to be 1.8 and the minor radius was adjusted until good impedance matching was obtained at the center frequency of the desired lower band, 0.915 GHz. This resulted in an ellipse with a semi-minor axis of 31 mm.

This design was simulated using the finite-element based full-wave 3D electromagnetic solver Ansys High Frequency Simulation Software (HFSS) [38]. The results for impedance matching, shown in Fig. 3.2, give a return loss of 15.5 dB at 0.915 GHz. The 10 dB impedance bandwidth is 298 MHz for a fractional bandwidth of

approximately 32.5%. The gain pattern, shown in Fig. 3.3, displays a forward gain of 6.0 dBi; the front-to-back ratio can be seen to be quite poor however at only 2.4 dB. Looking at the current distribution on the surfaces of the filled dipole in Fig. 3.4, we can see that the current is primarily concentrated along the outer edge of the elliptical arms, mirroring the result observed by Durgun *et al.* for the filled bow-tie antenna [19]. Therefore, we can proceed to an outline elliptical dipole antenna without sacrificing impedance matching or radiation performance.

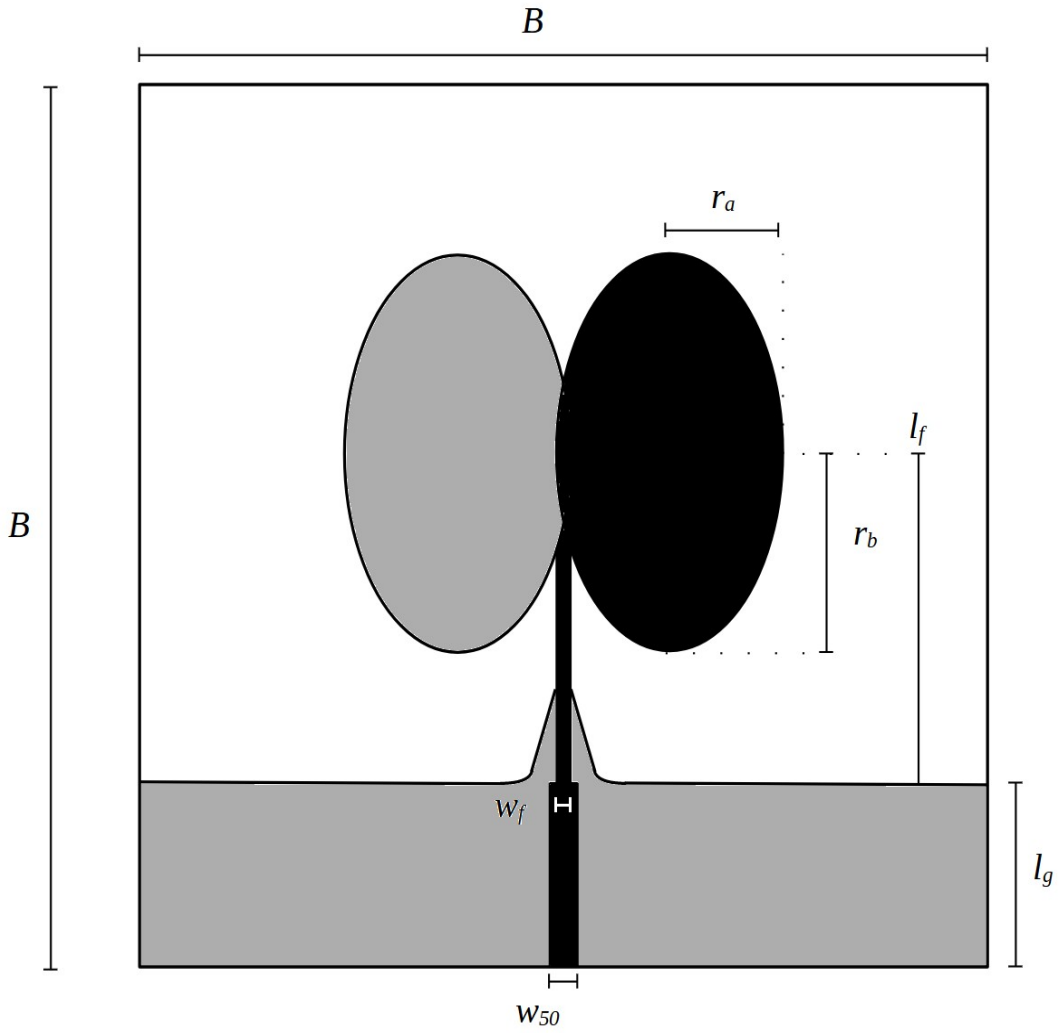

Fig. 3.1: Geometry of a single-band filled elliptical antenna with dimensions r_a = 31 mm and r_b = 55.8 mm. The top layer is shown in black and the bottom layer in gray. The antenna is fed by a 50 Ω microstrip line with w_{50} = 0.93 mm from a wave port excitation source to a feed line with l_f = 67.5 mm and w_f = 2 mm. The ground plane extends l_g = 22.5 mm with a linearly tapered, filleted section underneath the line. The substrate is Rogers Kappa 438 (ε_r = 4.38) with a thickness of 0.11 mm, and the board size (B) is 150 mm.

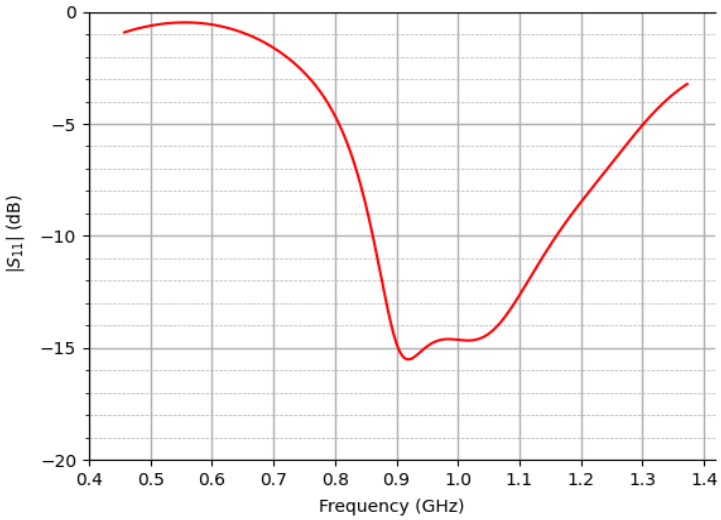

Fig. 3.2: Simulated $|S_{11}|$ versus frequency for the single-band filled elliptical dipole antenna.

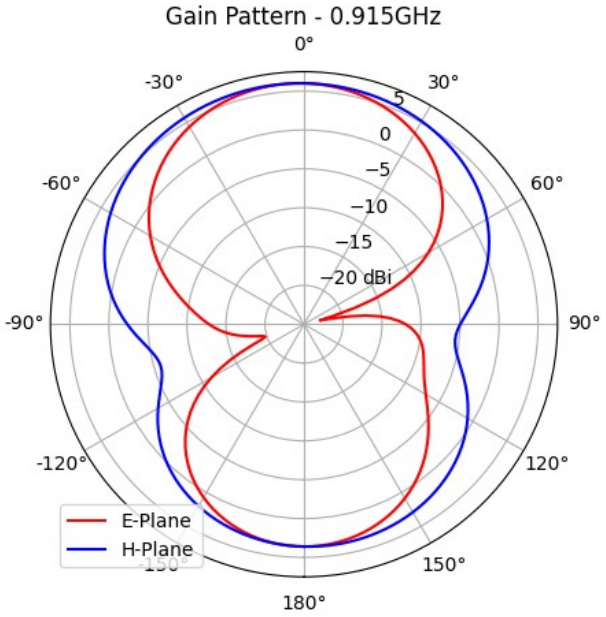

Fig. 3.3: Simulated E-plane (red) and H-plane (blue) radiation patterns at 0.915 GHz for the single-band filled elliptical dipole antenna.

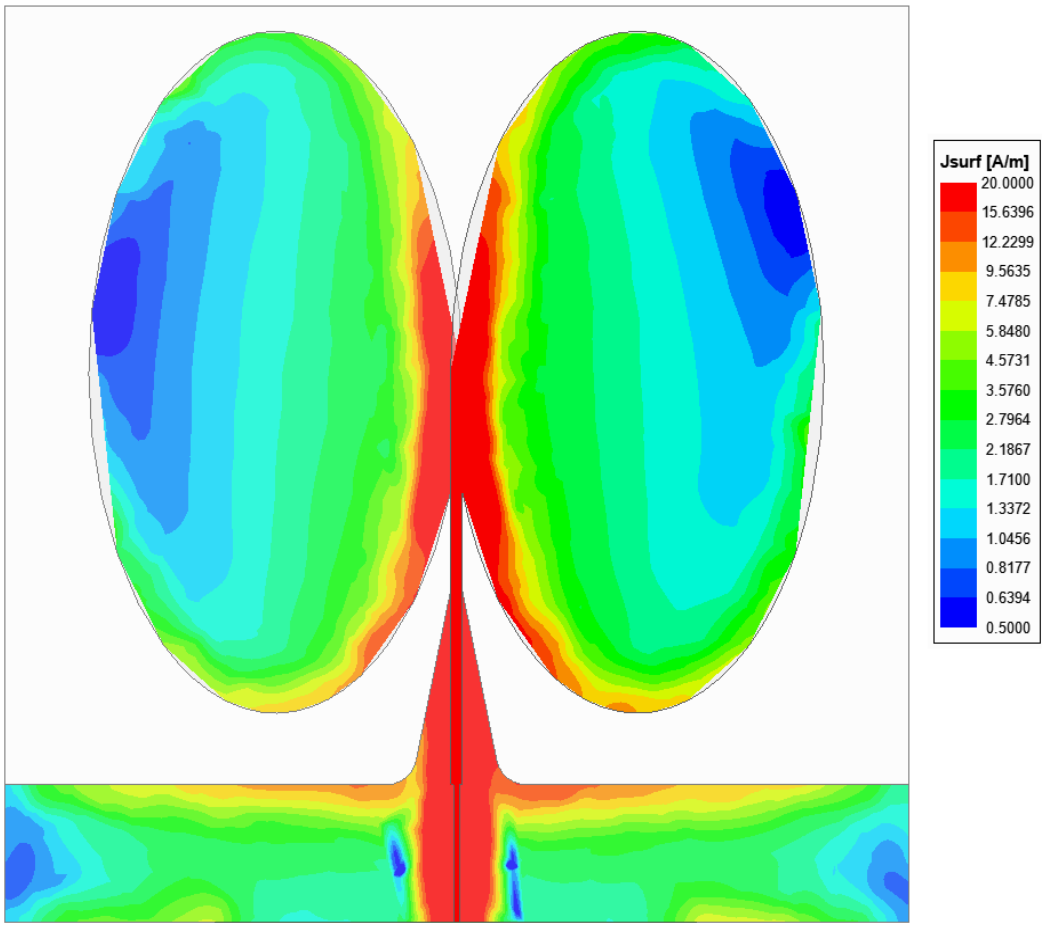

Fig. 3.4: Simulated surface current density at 0.915 GHz on the single-band filled elliptical dipole antenna.

3.2.2 Outline Elliptical Dipole

Having investigated the single-band filled elliptical antenna, we now turn our attention towards the single-band outline antenna. By removing the interior metallization from each of the elliptical arms, we can reduce weight and size while opening up space for a potential second set of antenna arms to operate at a higher frequency band. Fig. 3.5

shows the geometry of this outline antenna design.

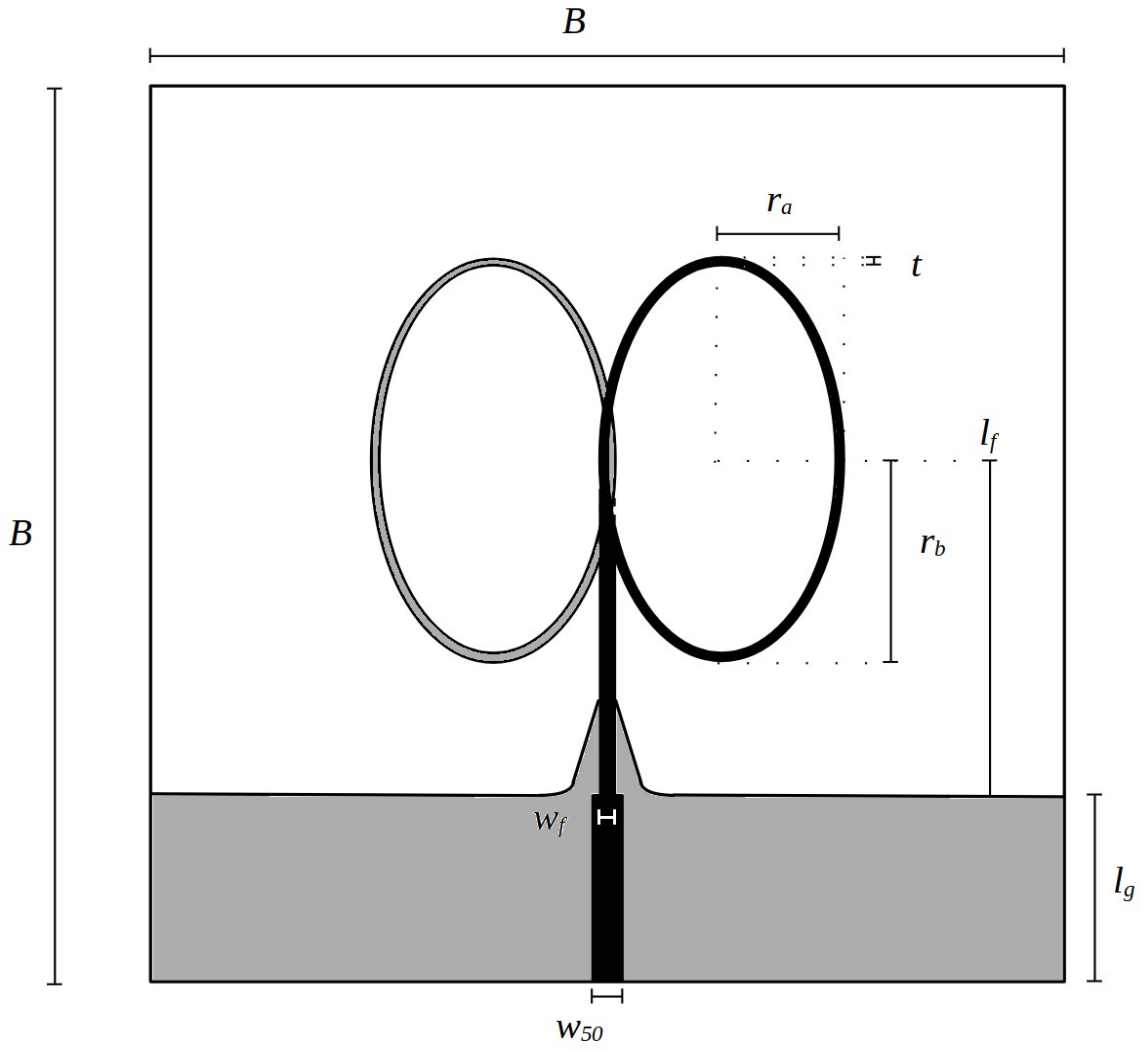

Fig. 3.5: Geometry of a single-band outline elliptical antenna. The top layer is shown in black and the bottom layer in gray. Two sets dimensions using this design are presented, one of the same size as the antenna presented in Fig. 3.1 and one tuned to operate at 0.915 GHz. The antenna is fed by a 50 Ω microstrip line with w_{50} = 0.93 mm. The substrate is Rogers Kappa 438 (ε_r = 4.38) with a thickness of 0.11 mm, and the board size (B) is 150 mm.

We begin by presenting an outline elliptical dipole with the same dimensions as the filled elliptical dipole shown in Fig. 3.1. This antenna has dimensions r_a = 31 mm, r_b = 55.8 mm, t = 0.75 mm, w_f = 2 mm, l_f = 67.5 mm, and l_g = 22.5 mm. A comparison of

the return loss for the filled antenna and the outline antenna is shown in Fig. 3.6. This shows that removing the interior metallization shifted the resonant frequency from 0.915 GHz down to 0.636 GHz and results in a narrower bandwidth. The impedance matching at the resonant frequency is still satisfactory, however. Fig 3.7 shows a radiation pattern comparison between the filled and outline antennas, displaying that the peak gain is slightly lower but still about 3.5 dBi, an acceptable value.

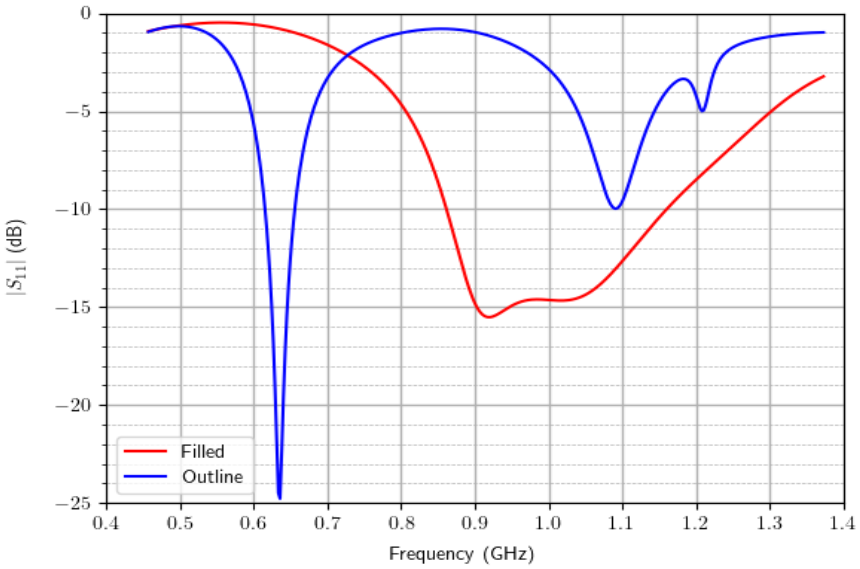

Fig. 3.6: Simulated $|S_{11}|$ versus frequency for the single-band filled elliptical dipole antenna shown in Figure 3.1 and a similarly-sized outline elliptical dipole shown in Fig. 3.5.

We now tune the outline antenna design of Fig. 3.5 to perform at 0.915 GHz. This gives the following dimensions: $r_a = 21.5$ mm, $r_b = 38.7$ mm, $t = 1$ mm, $w_f = 2$ mm, $l_f = 57.5$ mm, and $l_g = 40$ mm. The corresponding simulated $|S_{11}|$ result is plotted in Fig. 3.8.

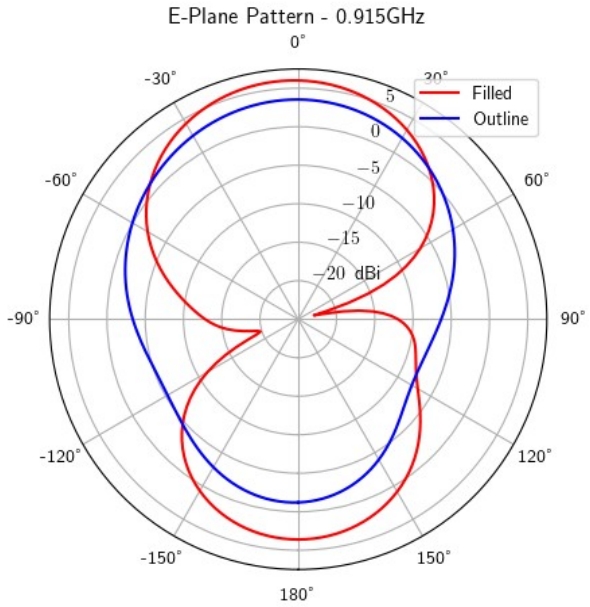

(a)

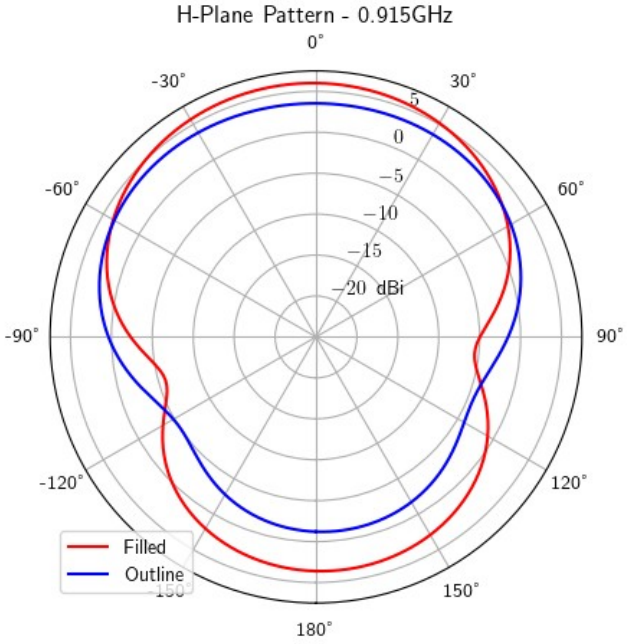

(b)

Fig. 3.7: Simulated (a) E-plane and (b) H-plane radiation patterns at 0.915 GHz for the single-band filled elliptical dipole antenna shown in Figure 3.1 and a similarly-sized outline elliptical dipole shown in Fig. 3.5.

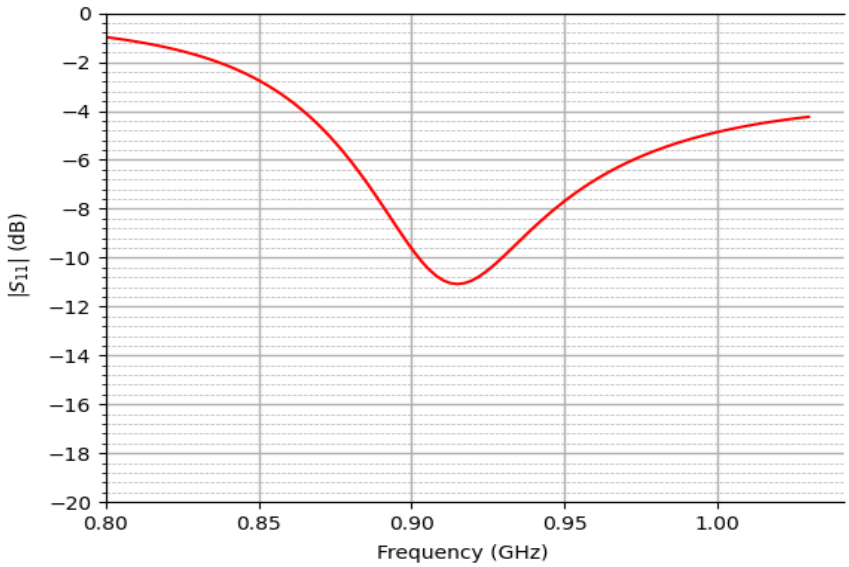

Fig. 3.8: Simulated $|S_{11}|$ versus frequency for the single-band outline elliptical dipole antenna shown in Fig. 3.5 tuned to 0.915 GHz.

The impedance matching curve in Fig. 3.8 reveals that the resonant frequency is indeed positioned at the same frequency as that of the filled antenna, 0.915 GHz. The semi-minor axis of the outline antenna is considerably smaller: 21.5 mm compared to 31 mm for the filled antenna, approximately a one-third reduction in that dimension. Since the eccentricity of each antenna is the same, that reduction is also seen in the major axis dimension. As expected then, removing the interior metallization provides compactness at the expense of impedance bandwidth.

E-plane and H-plane cuts of the radiation pattern for this design are shown in Fig. 3.9. This shows a peak gain of 5.85 dBi, which is quite close to the filled design, and a front-to-back ratio of 3.4 dB, which is about a 1 dB improvement over the filled elliptical antenna.

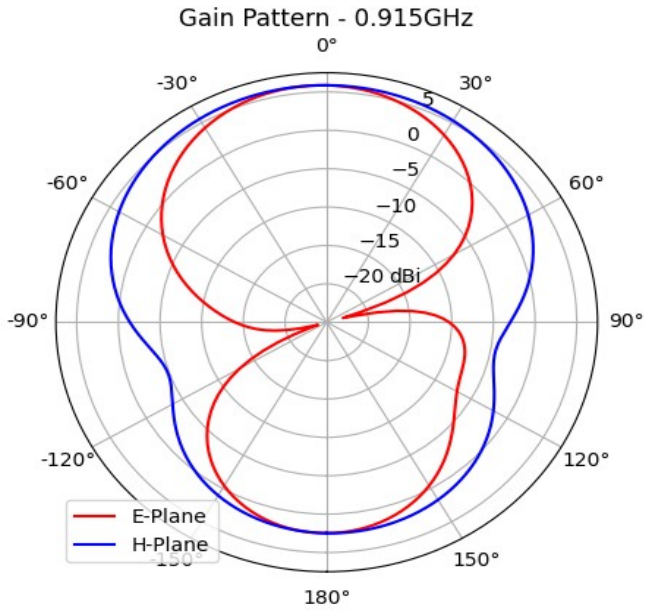

Fig. 3.9: Simulated E-plane (red) and H-plane (blue) radiation patterns at 0.915 GHz for the single-band outline elliptical dipole antenna.

3.3 Dual-band Antennas

3.3.1 Inset Antenna Arms

To achieve dual-band operation for this antenna, we add a second set of outline elliptical (circular in this case) antenna arms within the space hollowed out in the outline antenna from Fig. 3.5 [39]. This results in an “inset” dual-band design as shown in Fig. 3.10.

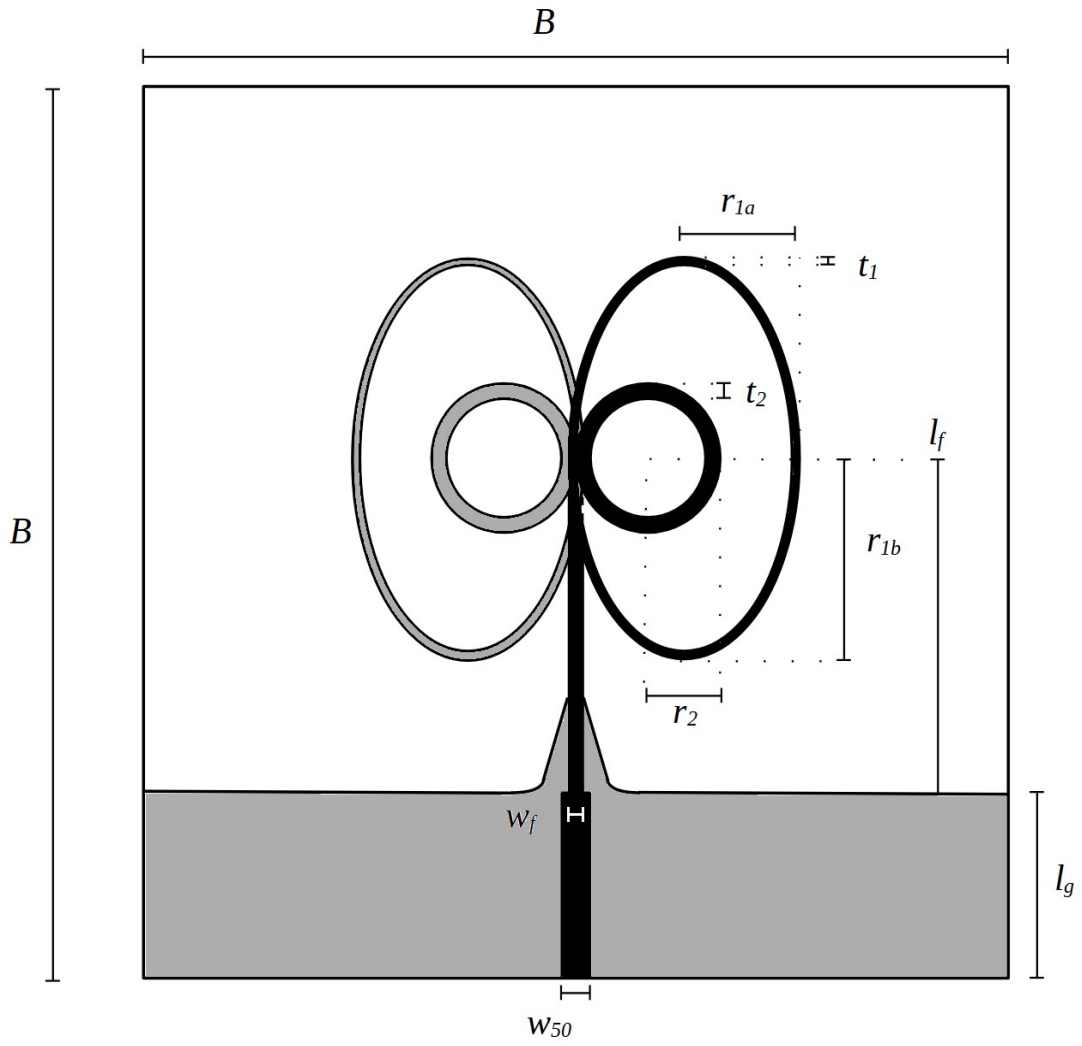

Fig. 3.10: Geometry of a dual-band inset elliptical antenna with dimensions r_{1a} = 21.5 mm, r_{1b} = 38.7 mm, r_2 = 9.8 mm, t_1 = 1 mm, and t_2 = 0.4 mm. The top layer is shown in black and the bottom layer in gray. The antenna is fed by a 50 Ω microstrip line with w_{50} = 0.93 mm connected to a feed line with l_f = 57.5 mm and w_f = 2 mm. The ground plane extends l_g = 40 mm. The substrate is Rogers Kappa 438 (ε_r = 4.38) with a thickness of 0.11 mm, and the board size (B) is 150 mm.

The impedance matching in each band for this antenna is shown in Fig. 3.11. It can be seen that resonant frequency in the lower band is unaffected by the addition of the interior, upper-band arms and the return loss is nearly 15 dB. Due to the strong electromagnetic coupling between such closely-spaced arms, the upper band, however, is not well matched. To mitigate this, decoupling elements will be added to help improve

the impedance matching.

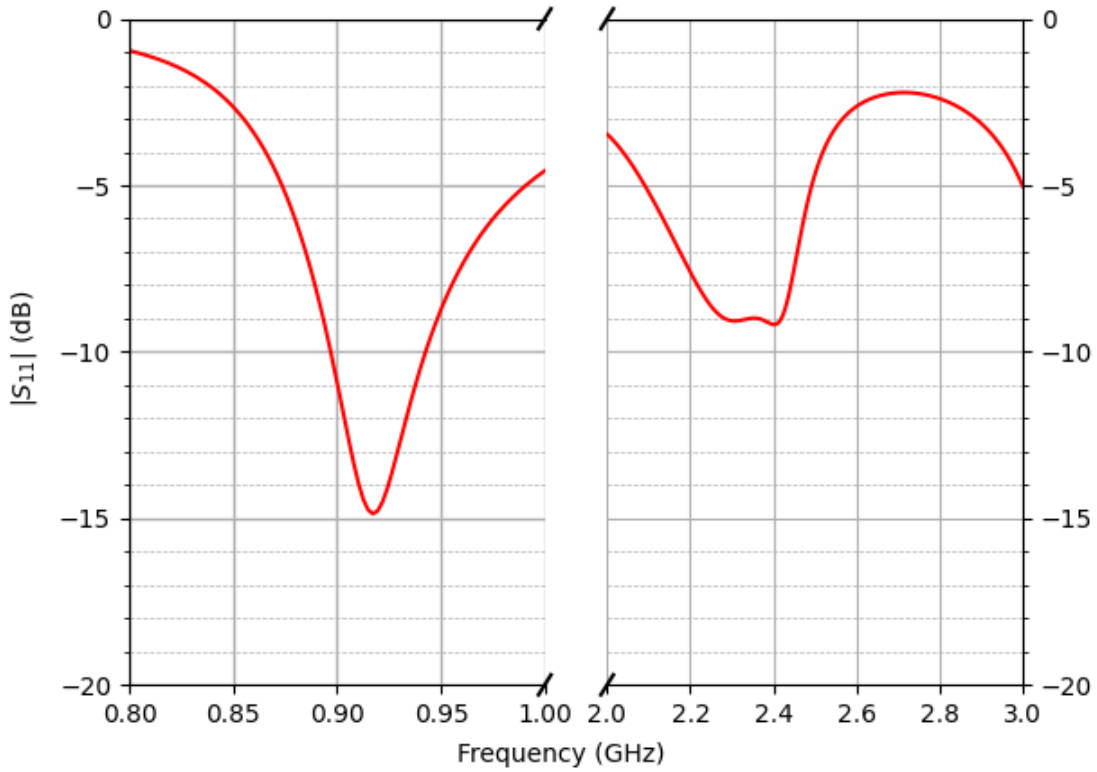

Fig. 3.11: Simulated $|S_{11}|$ versus frequency for both the lower and upper bands for the dual-band inset antenna shown in Fig. 3.10.

The gain patterns at each band are plotted in Fig. 3.12. A comparison between Fig. 3.9 and Fig. 3.12a reveals nearly identical performance at 0.915 GHz, once again showing the insensitivity of the lower-band performance to additional elements within the lower-band arm. The upper-band characteristics shown in Fig. 3.12b are adversely impacted by the coupling of the arms, resulting in a lower peak gain of 1.47 dBi and only 2.49 dB of front-to-back ratio. It was observed that changing the lower-band arm

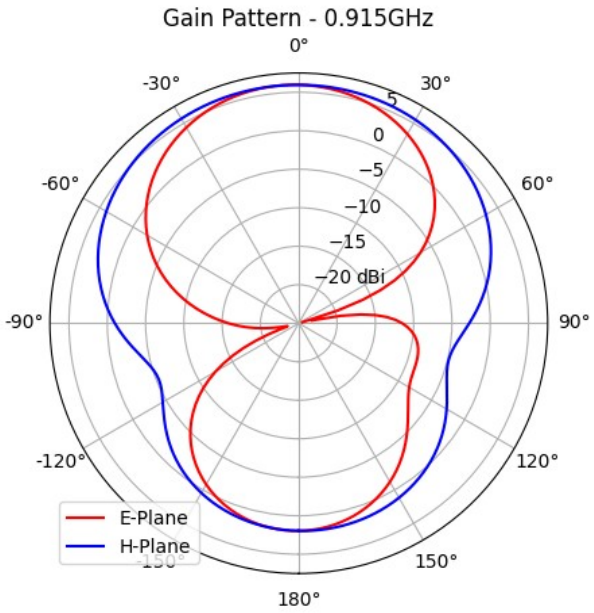

(a)

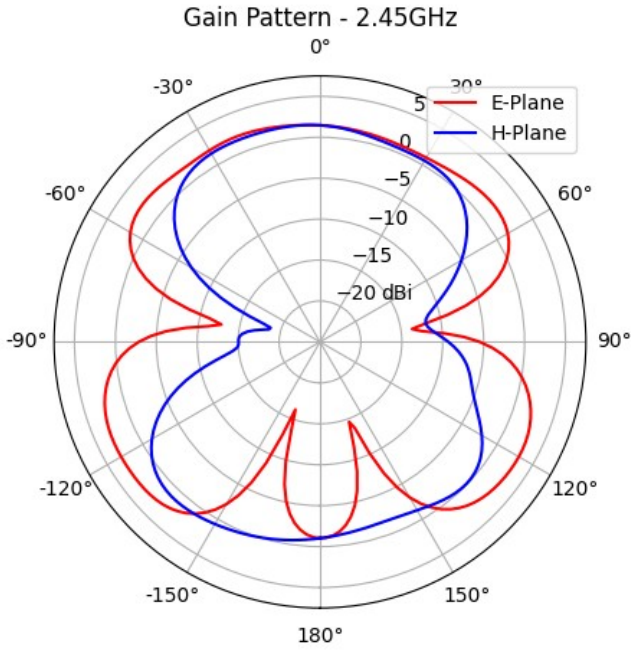

(b)

Fig. 3.12: Simulated E-plane (red) and H-plane (blue) radiation patterns at (a) 0.915 GHz and (b) 2.45 GHz for the dual-band inset antenna shown in Fig. 3.10.

geometry profoundly altered the upper-band performance via mutual coupling. As such, methods of reducing this mutual coupling behavior were investigated.

3.3.2 Opposed Antenna Arms

In an attempt to mitigate the effects of mutual coupling between the antenna arms, the upper-band arm, which is inside the lower-band arm in Fig. 3.10, was reflected across the antenna feed to produce the "opposed" antenna design shown in Fig. 3.13. This will in turn introduce a 180° phase reversal in the surface current distributions to help reduce the mutual coupling between the arms.

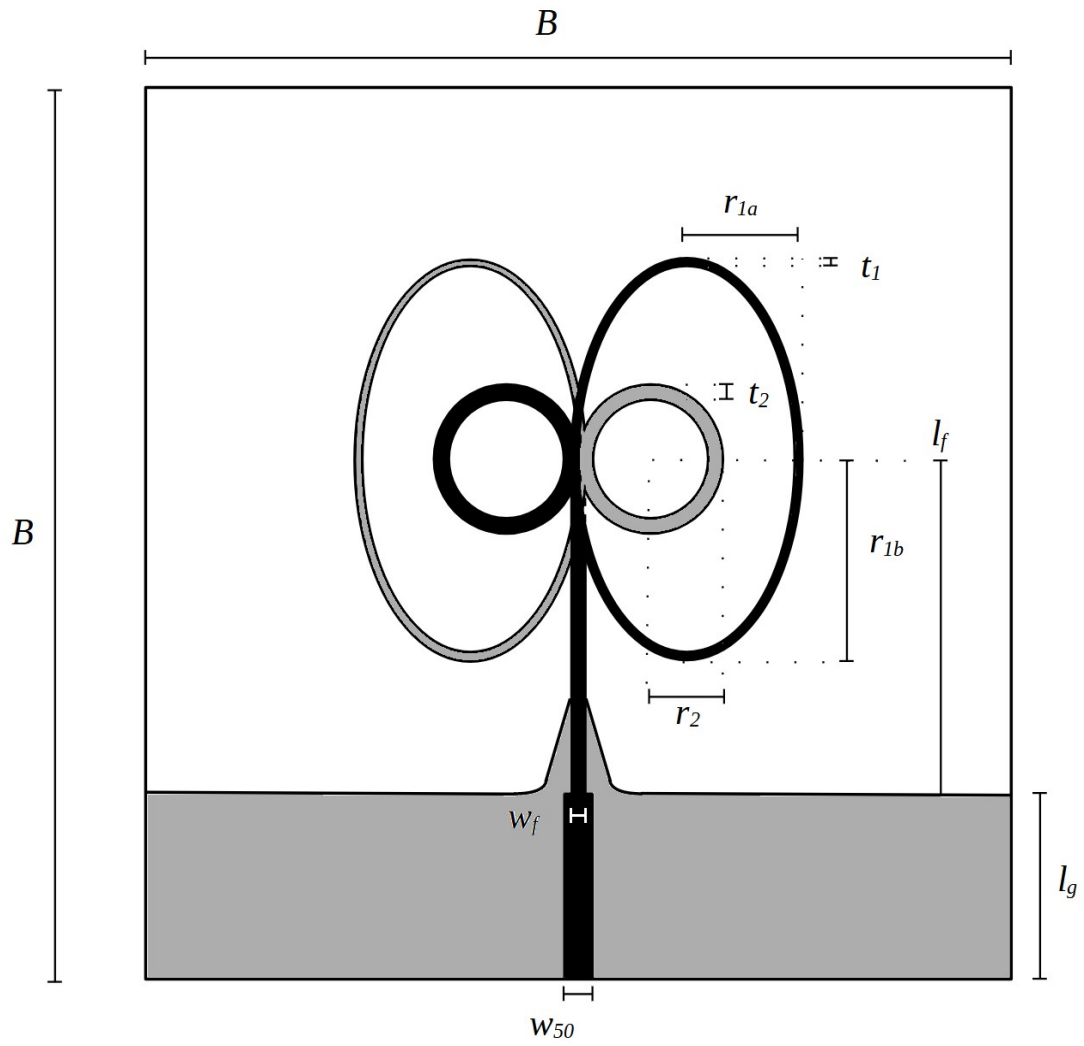

Fig. 3.13: Geometry of a dual-band opposed elliptical antenna with dimensions r_{1a} = 22 mm, r_{1b} = 39.6 mm, r_2 = 9.8 mm, t_1 = 0.2 mm, and t_2 = 0.4 mm. The top layer is shown in black and the bottom layer in gray. The antenna is fed by a 50 Ω microstrip line with w_{50} = 0.93 mm connected to a feed line with l_f = 57.5 mm and w_f = 0.5 mm. The ground plane extends l_g = 40. The substrate is Rogers Kappa 438 (ε_r = 4.38) with a thickness of 0.11 mm, the board size (B) is 150 mm.

The S_{11} performance of this antenna in each band is shown in Fig. 3.14. The lower-band performance is slightly worse than that of the inset antenna, but the upper-band return loss is significantly improved. The resonant frequency of this antenna is 2.58

GHz, higher than is desired, and tuning the upper-band resonant frequency was still quite challenging.

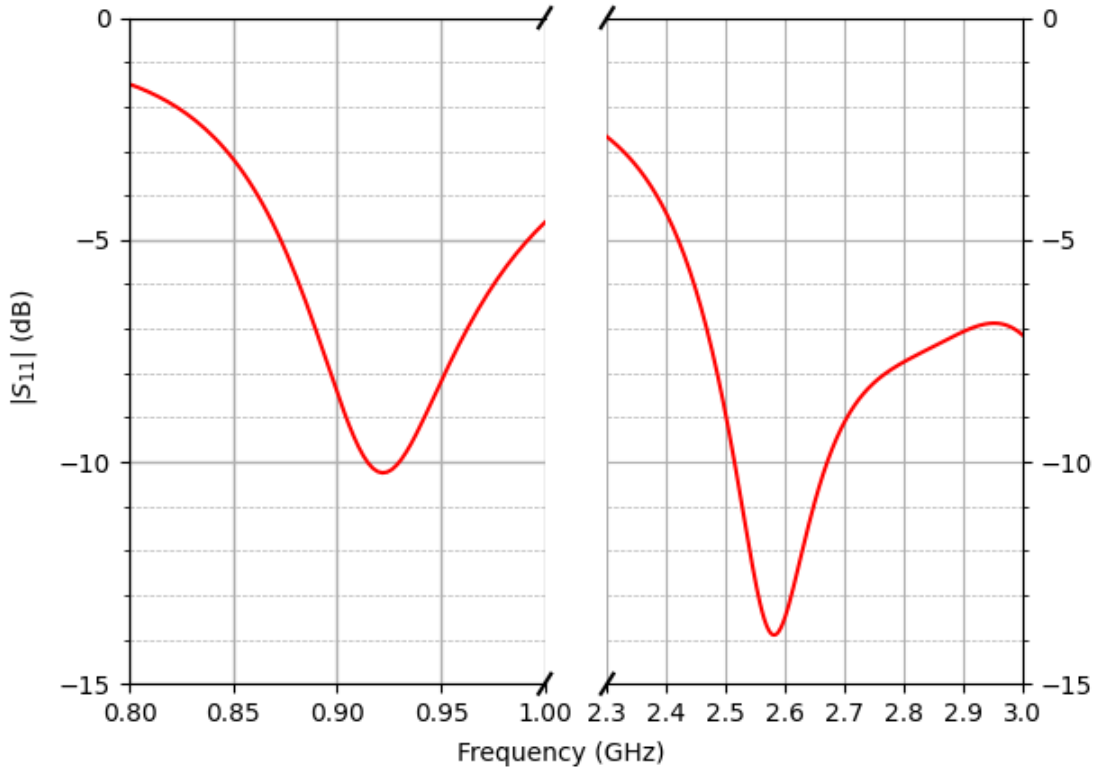

Fig. 3.14: Simulated $|S_{11}|$ versus frequency for both the lower and upper bands for the dual-band opposed antenna shown Fig. 3.13.

The radiation patterns for the opposed antenna are shown in Fig. 3.15. The lower-band radiation characteristics are similar to the inset antenna, but an additional 1.2 dB peak gain is seen in the upper band for a total of 2.67 dBi.

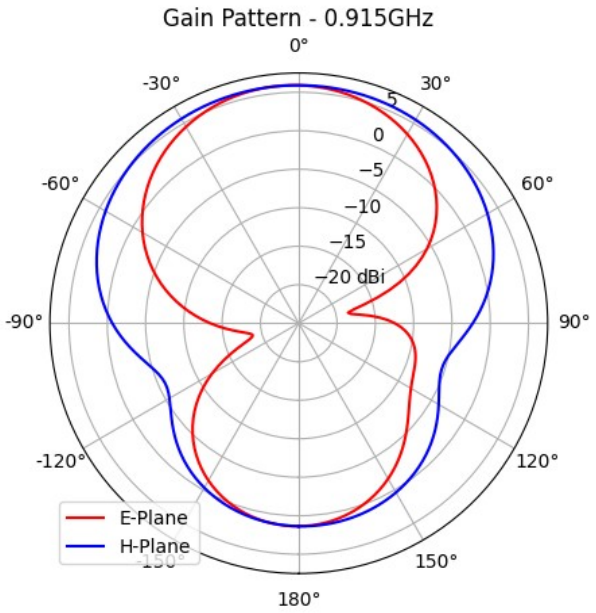

(a)

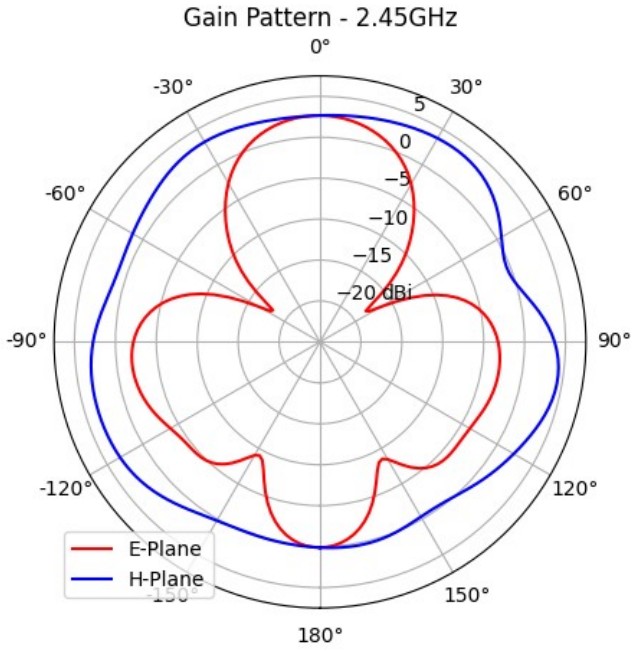

(b)

Fig. 3.15: Simulated E-plane (red) and H-plane (blue) radiation patterns at (a) 0.915 GHz and (b) 2.45 GHz for the dual-band opposed antenna shown Fig. 3.13.

The radiation pattern at the lower-band was found to be sensitive to the size of the ground plane. In order to sufficiently suppress the back lobe in the lower-band with an acceptable preliminary board size of 150 mm in each dimension, the ground plane was given an exponential taper up the sides of the PCB which extended to be in line with the feed point, as shown in Fig. 3.16.

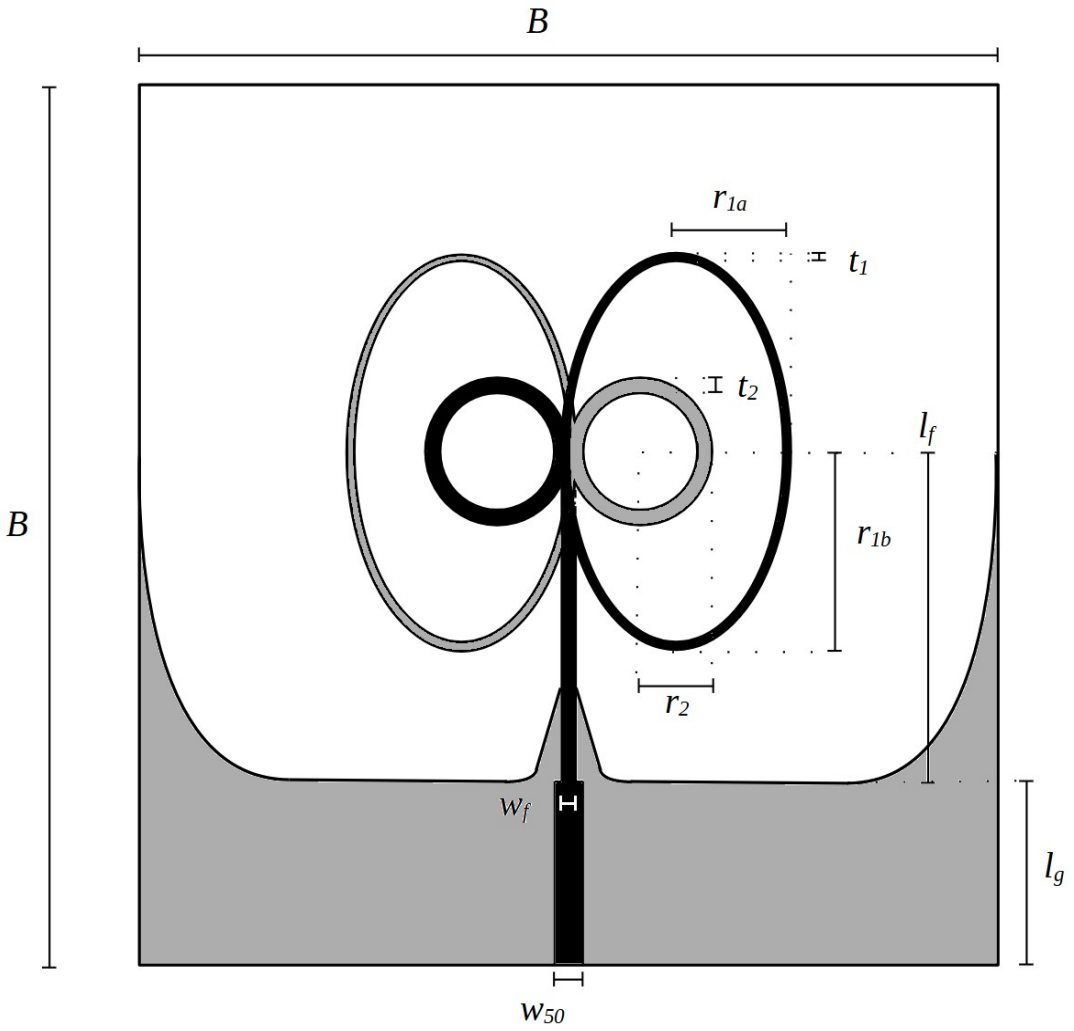

Fig. 3.16: Geometry of a dual-band elliptical antenna with extended ground having dimensions r_{1a} = 22 mm, r_{1b} = 39.6 mm, r_2 = 9.8 mm, t_1 = 0.2 mm, and t_2 = 0.4 mm. The top layer is shown in black and the bottom layer in gray. The antenna is fed by a 50 Ω microstrip line with w_{50} = 0.93 mm connected to a feed line with l_f = 57.5 mm and w_f = 0.5 mm. The ground plane extends l_g = 40 mm with an exponential taper. The substrate is Rogers Kappa 438 (ε_r = 4.38) with a thickness of 0.11 mm, and the board size (B) is 150 mm.

The benefits of this extended ground plane are highlighted in comparison to the antenna in Fig. 3.13. The S_{11} characteristics shown in Fig. 3.17 reveal that extending the ground plane assists with impedance matching in the lower band. The radiation patterns at 0.915 GHz and 2.45 GHz are shown in Figs. 3.18 and 3.19. While the performance in the upper band is almost unaffected by the addition of the exponential tapers, Fig. 3.18 exhibits a drastic difference in the lower-band radiation. The peak gain is slightly compromised, dropping to 3.37 dBi compared to 5.91 dBi for the antenna with no ground extension. This penalty is offset by the massive difference in the front-to-back ratio; 11.96 dB with the tapered ground compared to just 4.55 dB without.

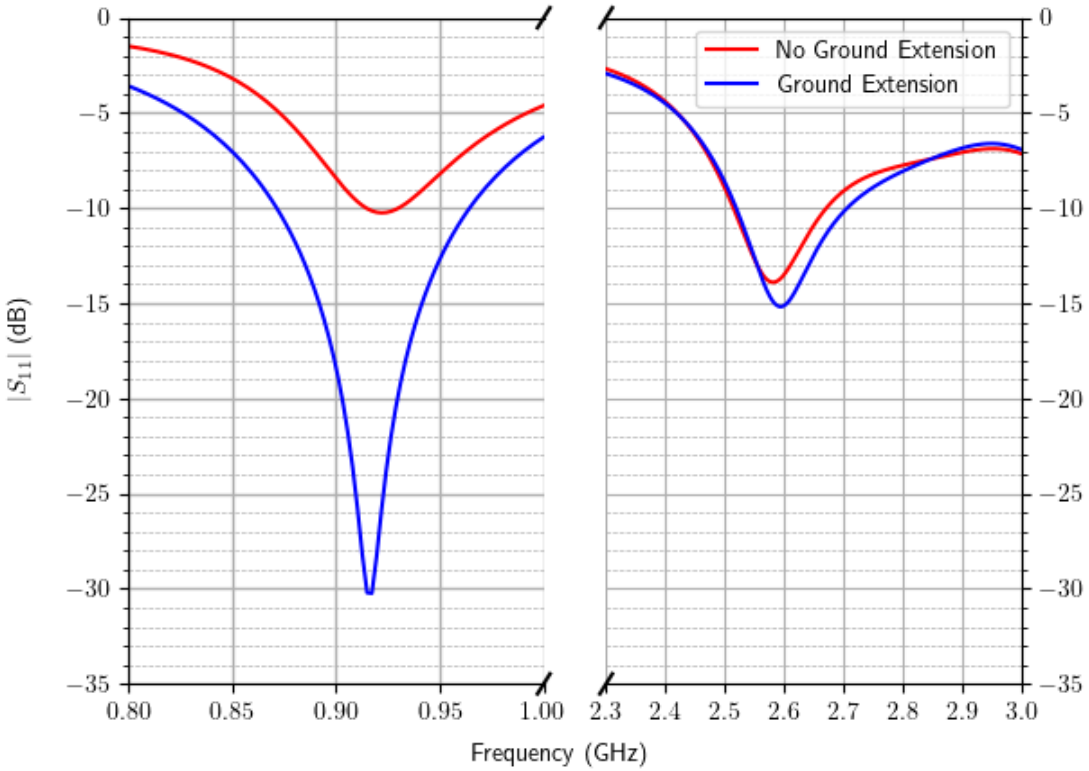

Fig. 3.17: Comparison of simulated $|S_{11}|$ versus frequency in both the lower and upper bands for the antenna with (Fig. 3.16) and without (Fig. 3.13) an extended ground plane.

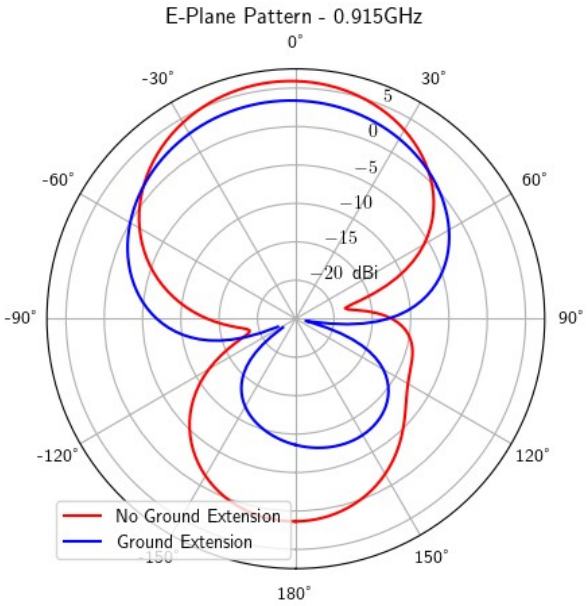

(a)

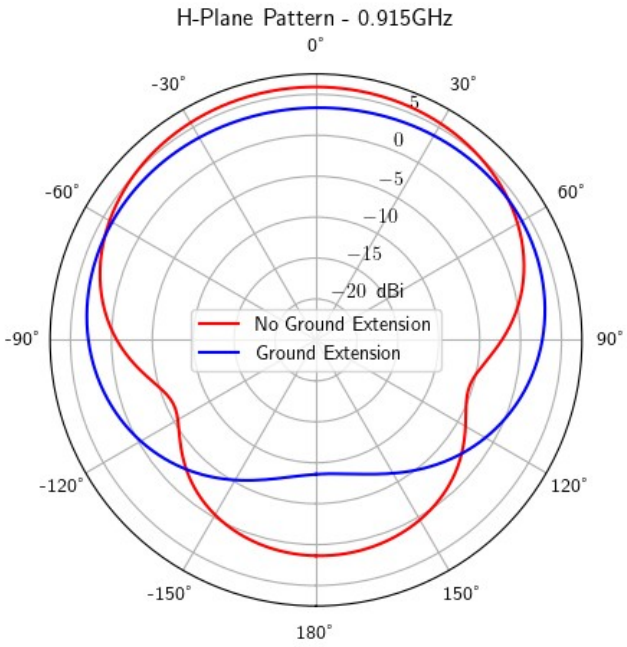

(b)

Fig. 3.18: Comparison of (a) E-plane and (b) H-plane radiation patterns at 0.915 GHz for the antenna with and without the extended ground plane.

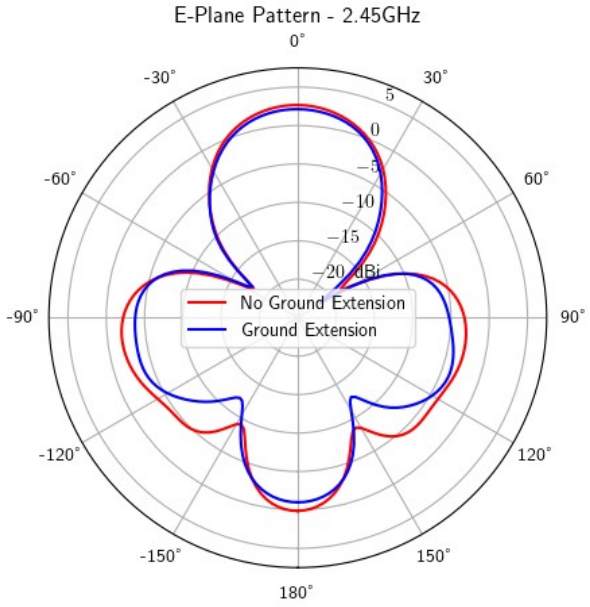

(a)

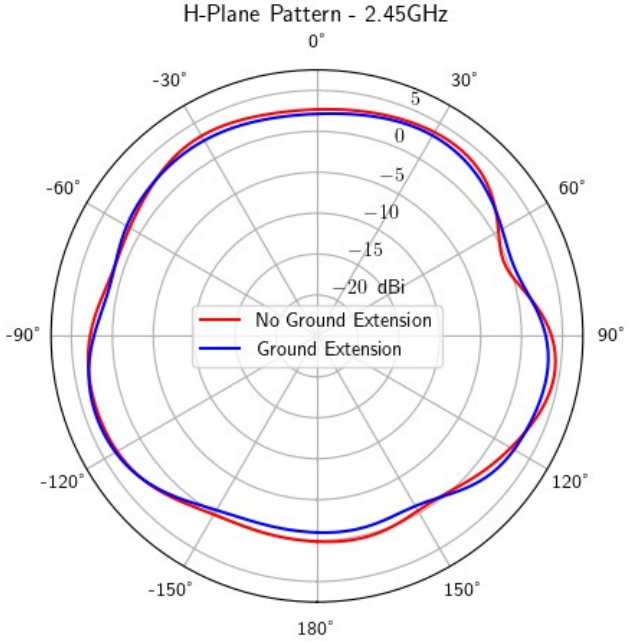

(b)

Fig. 3.19: Comparison of (a) E-plane and (b) H-plane radiation patterns at 2.45 GHz for the antenna with and without the extended ground plane.

3.3.4 Antenna with Additional Elements

To achieving good performance in all areas, we must then adjust the resonant frequency in the upper band and improve the front-to-back ratio at 2.45 GHz. Initially, promising results in accomplishing the latter were seen by adding reflective elements behind the upper-band antenna arms. The final step of tuning the resonant frequency, as well as improving suppression of the back lobe, was seen by adding curved parasitic elements inside of the lower-band arms. These elements help to further isolate the upper-band arms from the effects of mutual coupling with the lower-band arms. The final proposed antenna design is shown in Fig. 3.20.

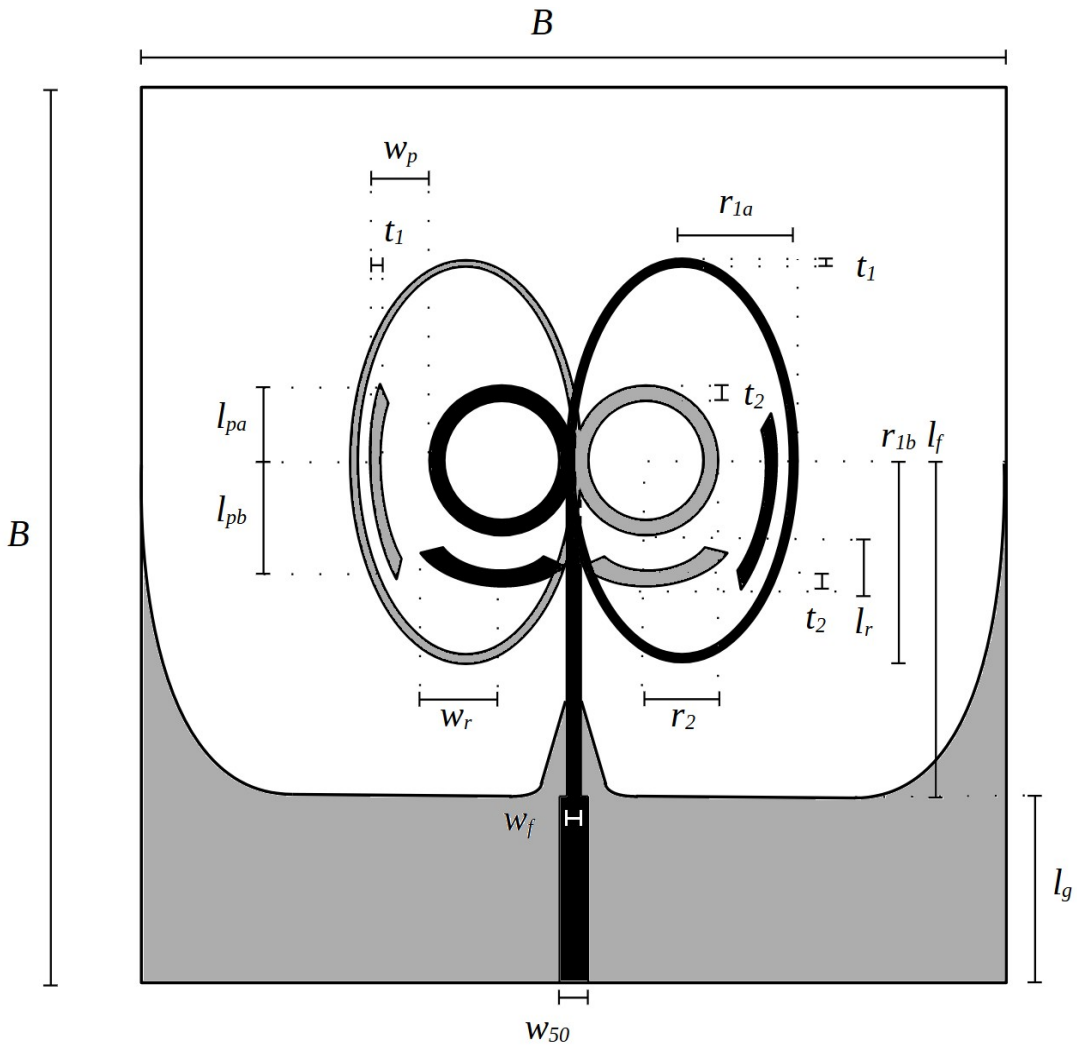

Fig. 3.20: Geometry of a dual-band elliptical antenna with dimensions r_{1a} = 22 mm, r_{1b} = 39.6 mm, r_2 = 9.8 mm, t_1 = 0.2 mm, and t_2 = 0.4 mm. The top layer is shown in black and the bottom layer in gray. The antenna has reflectors behind the upper-band arms; these are circular sections concentric with the upper-band arms with radii $r_2 + l_r$ where l_r = 10 mm. The reflectors are defined only within the outer ellipse and extend outward by w_r = 24.5 mm. There are also parasitics 2.2 mm inside and concentric with the lower-band arms with l_{pa} = 15mm and l_{pb} = 25 mm. The antenna is fed by a 50 Ω microstrip line with w_{50} = 0.93 mm connected to a feed line with l_f = 57.5 mm and w_f = 0.5 mm. The ground plane extends l_g = 40 mm with an exponential taper at the sides of the board. The substrate is Rogers Kappa 438 (ε_r = 4.38) with a thickness of 0.11 mm, and the board size (B) is 150 mm.

The performance of this final antenna was found to be satisfactory in all aspects. To demonstrate the performance improvements due to these additional reflecting

and parasitic elements, the S_{11} and radiation characteristics are therefore presented by comparing the previous case with just an extended ground plane, an antenna with just reflectors, an antenna with just parasitics, and finally an antenna with both of these additional elements. Fig. 3.21 shows the impedance matching in each band; the lower-band results are all roughly similar, but the upper band shows differences. Clearly the addition of the parasitics does provide good shielding from the mutual coupling, giving rise to a dual-resonance behavior. The lower of these resonances corresponds to the upper-band element radius, while the higher resonance seems to roughly correspond to three times the lower-band resonance and is thus a result of the lower-band arm's influence. The reflector seemed to yield slightly improved return loss at the lower of these upper-band resonance.

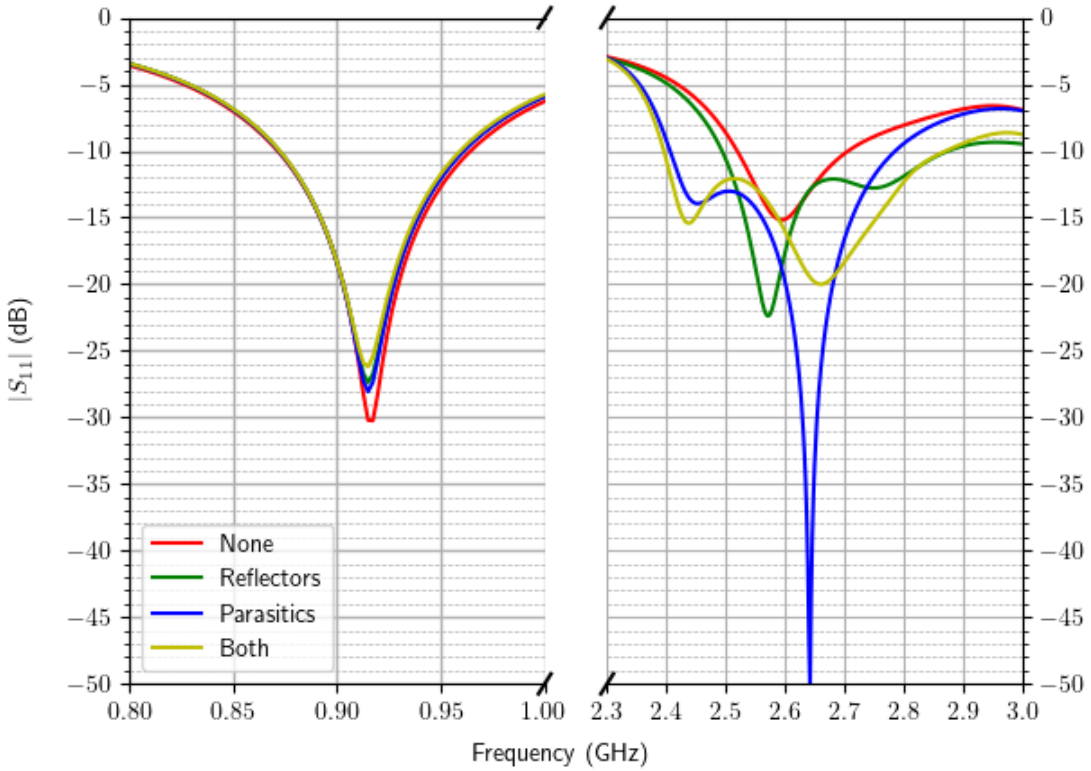

Fig. 3.21: Comparison of simulated $|S_{11}|$ versus frequency in both the lower and upper bands for the antenna with reflectors behind the upper-band arms, the antenna with parasitics inside the lower-band arms, neither of these additional elements, and both of them.

The antenna radiation patterns in each band are plotted in Figs. 3.22 and 3.23. Fig. 3.22 shows very little difference in the lower-band radiation pattern in adding additional elements to the antenna. Fig. 3.23 reveals that once again, the parasitic elements provide significant performance improvement in the upper band.

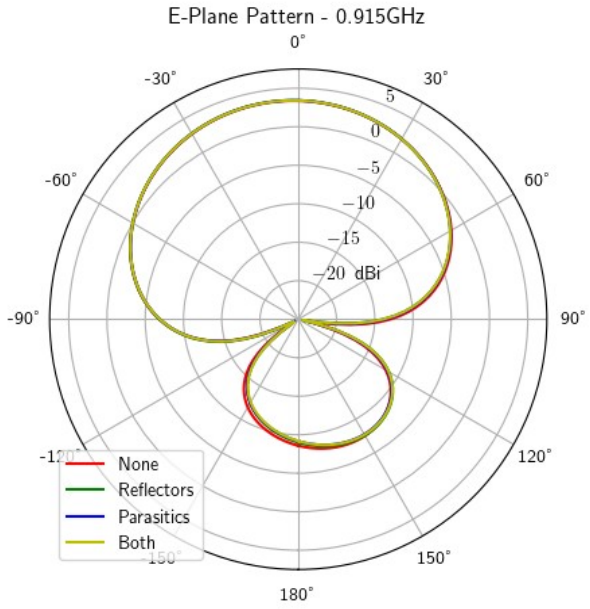

(a)

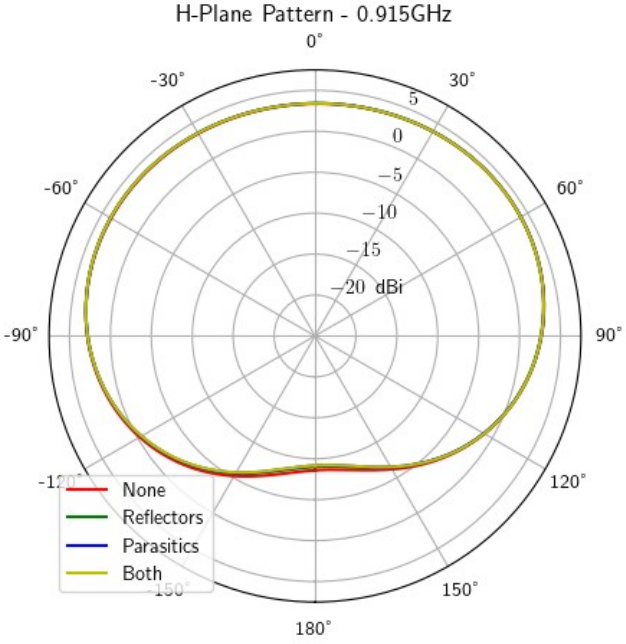

(b)

Fig. 3.22: Simulated E-plane (a) and H-plane (b) radiation patterns at 0.915 GHz for the antenna with reflectors behind the upper-band arms, the antenna with parasitics inside the lower-band arms, neither of these additional elements, and both of them.

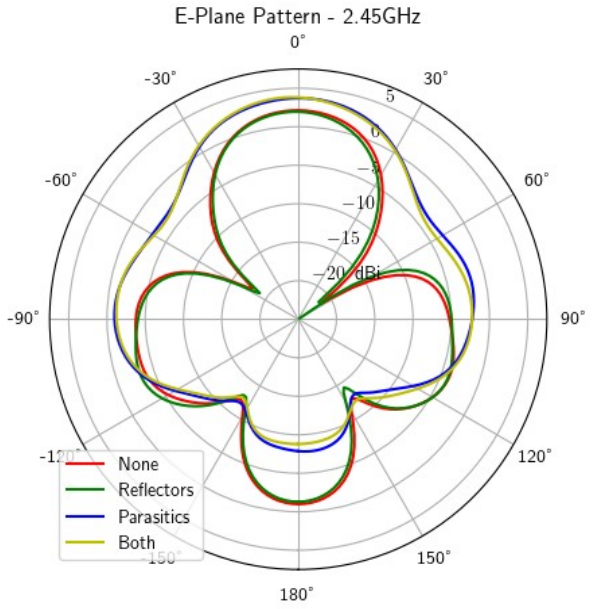

(a)

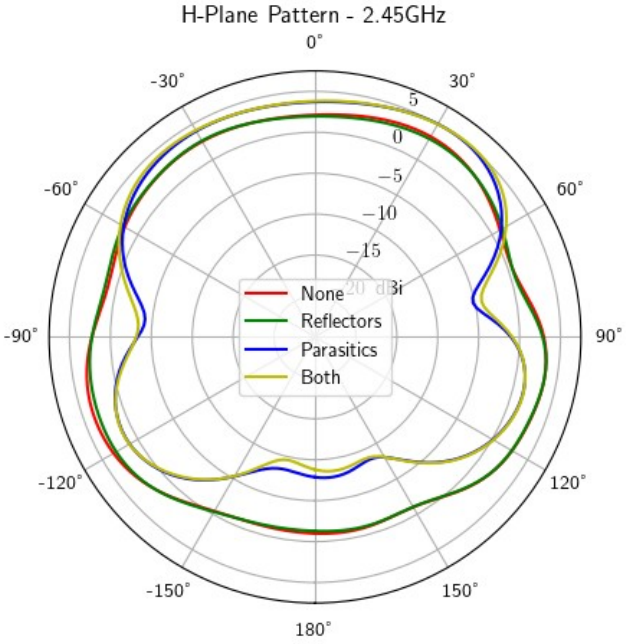

(b)

Fig. 3.23: Simulated E-plane (a) and H-plane (b) radiation patterns at 2.45 GHz for the antenna with reflectors behind the upper-band arms, the antenna with parasitics inside the lower-band arms, neither of these additional elements, and both of them.

3.4 Summary

Chapter 3 presents the procedure by which the dual-band elliptical antenna was designed. The starting point, a single-band filled elliptical dipole, had its interior metallization removed to form an outline antenna, increasing compactness. An additional radiating element tuned to the upper band was placed within the outline antenna, but mutual coupling between the arms was detrimental to performance. This was improved slightly by reversing the relative phase through mirroring the upper-band arm across the feed in the opposed dual-band antenna. Back lobe suppression in the lower band was achieved through an exponential taper of the ground plane. Finally, adding additional elements in reflectors for the upper-band elements and parasitics for the lower-band elements improved impedance matching and front-to-back ratio in the upper band; most of this performance gain is due to the shielding provided by the parasitics.

CHAPTER 4

Parametric Investigation of the Proposed Dual-Band Antenna

4.1 Introduction

In addition to designing the dual-band antenna shown in Fig. 3.20, we carried out parametric sweeps on two aspects of the design: the semi-minor axis of the outer antenna arms and the exponential curvature of the extended ground plane. We also show a continuation of the design shown in Fig. 3.20 by reducing the size of the board to 120 mm by 120 mm. This 20% reduction in size in each dimension compared to the original design affects the front-to-back ratio of the antenna, necessitating the addition of another design element, quarter-wavelength choke slots within the partial ground plane. The corresponding results will be presented in this chapter.

4.2 Parametric Sweep of Semi-Major Axis

For the dual-band antenna shown in Fig. 3.20 the semi-major axis r_{1b} was 39.6 mm. To investigate the effect of the eccentricity of the outer ellipse on the performance of the antenna, a parametric sweep of r_{1b} was carried out. The eccentricity e is calculated using Eq. 4.1:

$$e = \sqrt{(1 - r_{1a}^2 / r_{1b}^2)}. \tag{4.1}$$

In addition to the case of r_{1b} = 39.6 mm discussed in Section 3.3.4, antennas with semi-major axis values of 35.2 mm and 44.0 mm were full-wave analyzed. For each of these cases, the semi-minor axis r_{1a} was held constant at 22 mm. Changing the semi-major axis therefore changed the value of r_{1b}: r_{1b} = 35.2 mm and r_{1b} = 44 mm. As shown in Fig. 4.1, the resonant frequency in the lower band varied significantly with the axial ratio.

It was noted during simulation that the lower band resonant frequency was roughly dependent on the circumference of the outer ellipse. Since we held the minor axis constant during this sweep, the axial ratio determined this circumference. This explains the higher resonant frequency of 0.970 GHz for r_{1b} = 35.2 mm and a lower resonant frequency of 0.862 GHz for r_{1b} = 44.0 mm. Furthermore, the cases of both r_{1b} = 35.2 mm and r_{1b} = 44.0 mm changed the return loss at their resonant frequencies to 17.54 dB and 14.17 dB, respectively, from 26.19 dB at 0.915 GHz for r_{1b} = 39.6 mm. Nonetheless, both return loss values are well above the 10 dB level. However, steps that were taken to

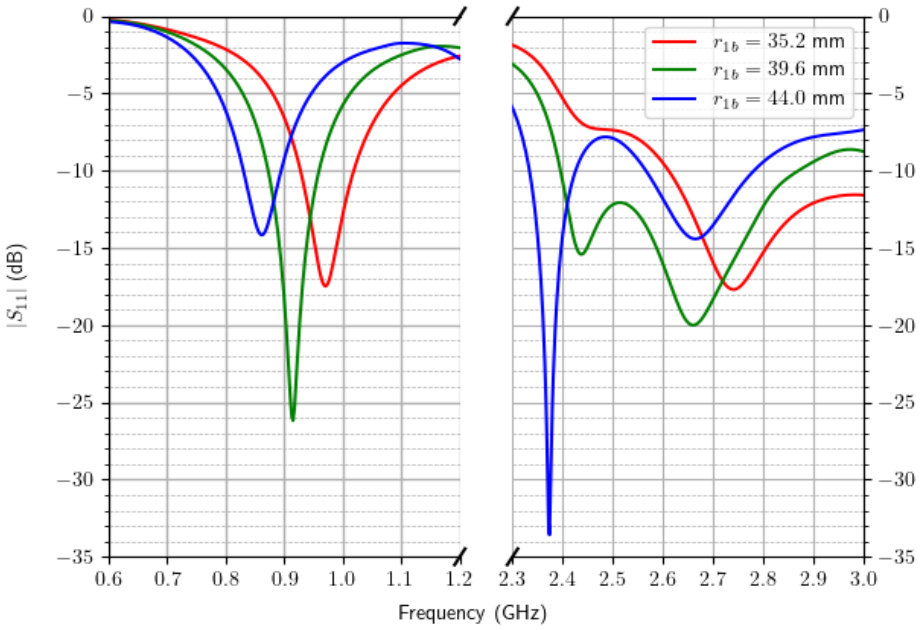

Fig. 4.1: Simulated $|S_{11}|$ versus frequency for both the lower and upper bands for several values of the outer ellipse semi-major axis.

improve impedance matching for the r_{1b} = 39.6 mm antenna such as tuning the antenna arm widths, t_1 and t_2, and the feed line width w_f were not undertaken for these other cases. The upper band return loss pattern for both the r_{1b} = 39.6 mm and r_{1b} = 44.0 mm cases shows a dual-resonance behavior, with the first of these resonances placed near the target frequency of 2.45 GHz. For the r_{1b} = 35.2 mm case, however, this first resonance is significantly suppressed and the 10 dB return loss band exists only at the higher end of that frequency range.

The gain patterns at both 0.915 GHz and 2.45 GHz are plotted in Figs. 4.2 and 4.3, respectively. Fig. 4.2 shows little variance across the cases, so the radiation pattern in that band seems to be insensitive to changes in the axial ratio. In all cases, the peak gain is roughly 3.5 dBi and the front-to-back ratio is within 0.5 dB of 12.1 dB.

The radiation patterns in the upper band shown in Fig. 4.3 display more change across these cases. The values for peak gain and front-to-back ratio for each case, as well as the lower-band resonant frequencies as shown in Fig. 4.1, are summarized in Table 4.1. The peak gain at 2.45 GHz increases with the semi-major axis, with a difference of 3.3 dB at the extreme cases. The back lobe is also more greatly attenuated at higher axial ratios with a swing of more than 6.5 dB. These performance gains are significant and could warrant designing the antenna to have a higher eccentricity.

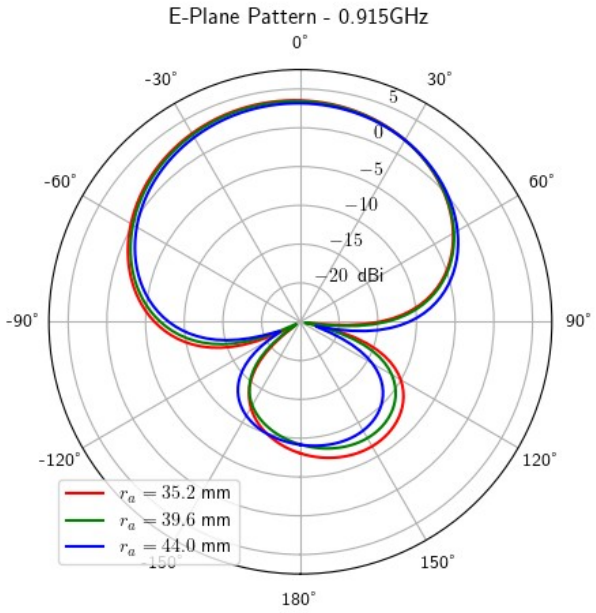

(a)

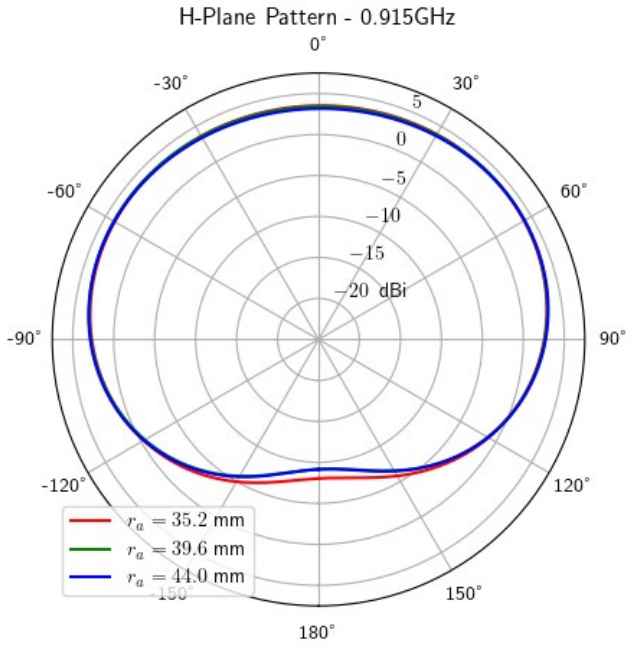

(b)

Fig. 4.2: Simulated E-plane (a) and H-plane (b) radiation patterns at 0.915 GHz for several values of the outer ellipse semi-major axis.

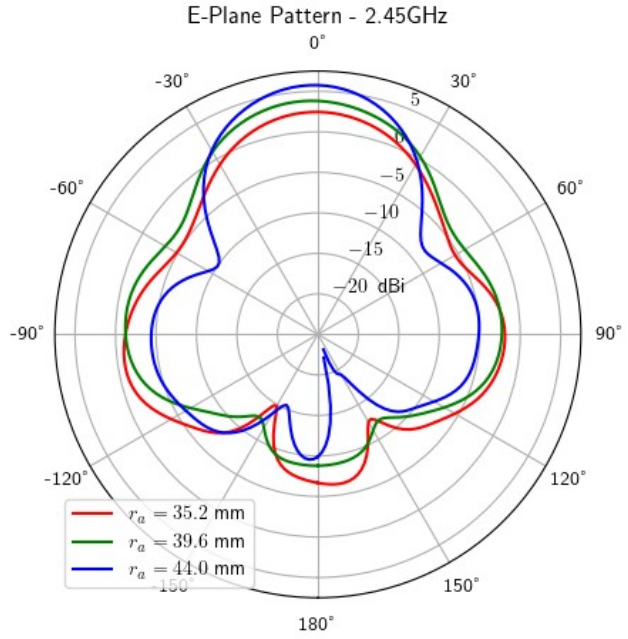

(a)

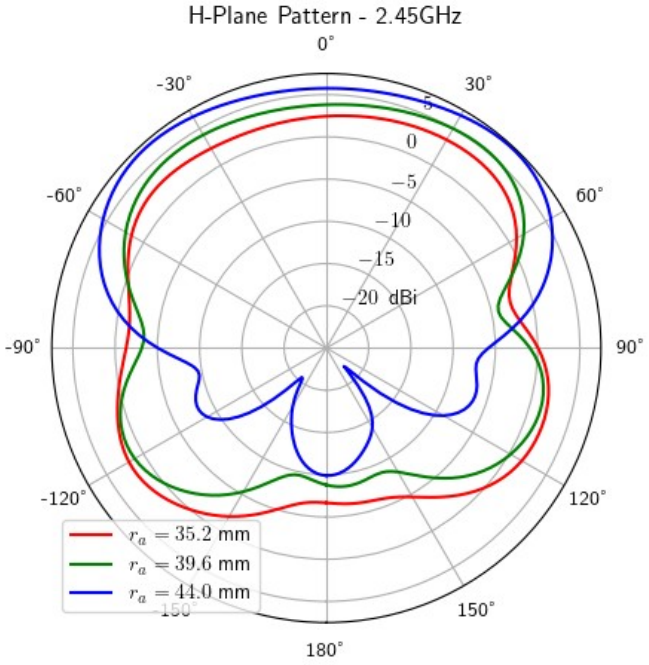

(b)

Fig. 4.3: E-plane (a) and H-plane (b) radiation patterns at 2.45 GHz for several values of the outer ellipse semi-major axis.

Table 4.1: Comparison of ellipse eccentricity, resonant frequency in the lower band, and peak gain and front-to-back ratio at 2.45 GHz over the sweep of r_{1b}.

	r_{1b} = 35.2 mm	r_{1b} = 39.6 mm	r_{1b} = 44 mm
Eccentricity (*e*)	0.781	0.831	0.866
Lower-band Resonant Frequency	0.970 GHz	0.915 GHz	0.862 GHz
Peak Gain at 2.45 GHz	2.45 dBi	3.82 dBi	5.76 dBi
Front-to-Back Ratio at 2.45 GHz	9.13 dB	12.6 dB	15.7 dB

4.3 Parametric Sweep of Ground Plane Curvature

As the dual-band antenna design incorporates an exponentially tapered ground plane at the sides of the board, we endeavored to characterize the effect of the curvature of this ground plane on the antenna performance. We use the following equation to define the exponential taper in which l_f and B are defined as in Fig. 3.20, y is a value ranging from $-B/2$ to $B/2$, and c is a coefficient that we vary in this analysis:

$$z = l_f * \exp\left(c * \left(|y| * \frac{B}{2} - 1\right) - 1\right). \tag{4.2}$$

The nominal case used for the manufactured antenna is that of $c = 12$. For this sweep, we additionally simulate the cases of $c = 4$, $c = 6$, and $c = 28$. The geometry of the ground plane tapers corresponding to these different values of c is shown in Fig. 4.4. We can see from Fig. 4.4 that the lower values of c correspond to a smoother curve that comes closer to the outer antenna arms, while the higher values of c mean a sharper upturn but more distance to the radiating lower-band elements. Values of c lower than 4 were not considered as the ground plane approaches and eventually intersects the outer antenna arm.

Fig. 4.5 shows the S_{11} performance of the antenna for the different curvatures

considered. We can see that the cases of c = 12, 20, and 28 are nearly identical, with only slightly better impedance matching from c = 28 around 2.65 GHz. The case of c = 4 differs somewhat, achieving peak resonance at 0.906 GHz rather than 0.915 GHz and showing 23.4 dB return loss there compared to the 26 – 30 dB of the other cases.

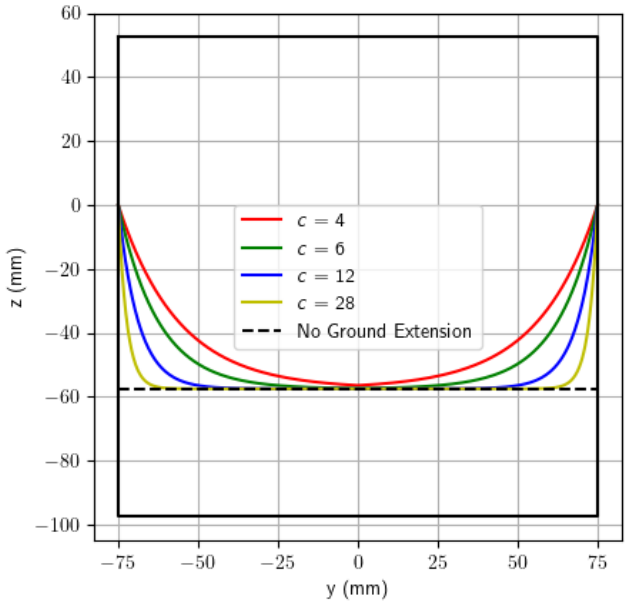

(a)

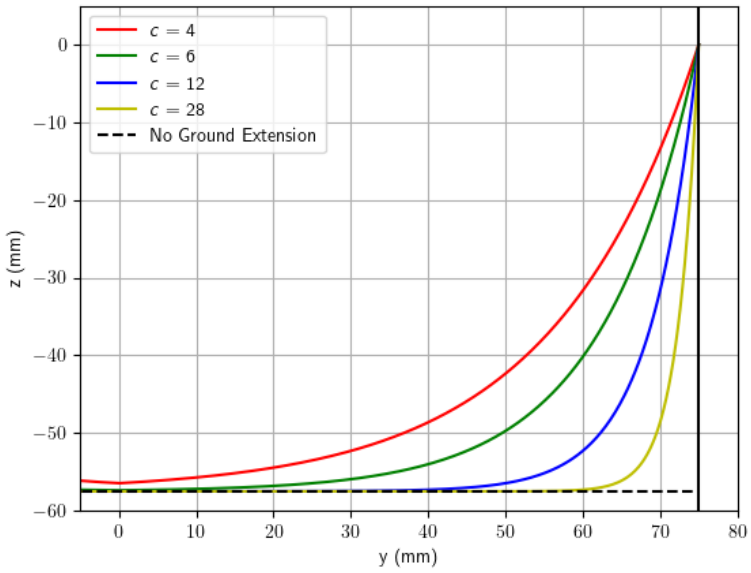

(b)

Fig. 4.4: Exponential tapers for the dual-band elliptical antenna, shown with the whole board outline in solid black (a) and at a closer view with the right edge of the board (b). The ground plane with no exponential taper is shown as a dashed black line. The curves for the exponential tapers are defined by Eq. (4.2) and the origin corresponds to the feed point of the antenna. Other features on the ground plane such as the filleted linear taper to the feed line are omitted in these diagrams.

Similarly, the E- and H-plane cuts of the pattern at 2.45 GHz are shown in Fig. 4.7. Once again we can observe that the H-plane patterns in Fig. 4.7b are nearly identical, but there is a slight difference in the E-plane pattern. It can be seen in Fig. 4.7a that the back lobe is more pronounced for the case $c = 4$, with nulls on either side of it. However, since we are most concerned with the characteristics of the antenna in the forward region, we can say that for our purposes, the radiation patterns of the antenna in both bands are unaffected by the range of curvatures we explored. It seems then that so long as ground plane is kept sufficiently far away from the elements as in the cases $c = 6$, 12, and 28, there will be no significant differences in antenna performance.

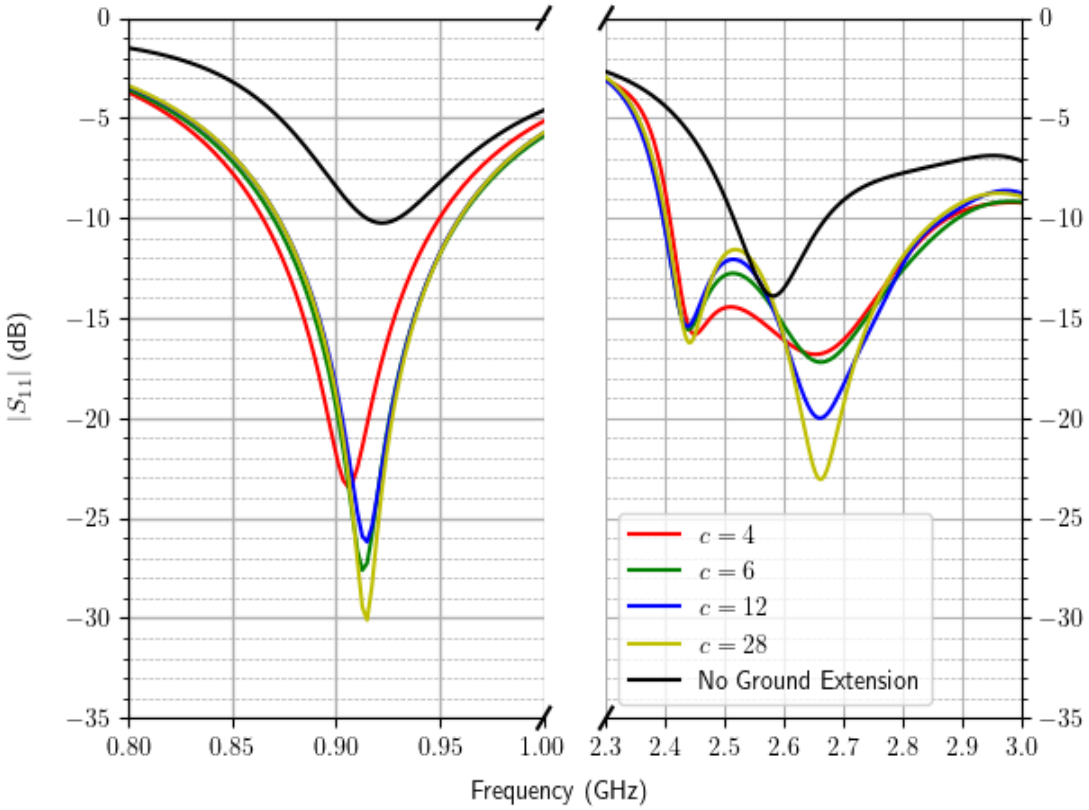

Fig. 4.5: Simulated $|S_{11}|$ versus frequency for both the lower and upper bands for a variety of values of the coefficient *c*.

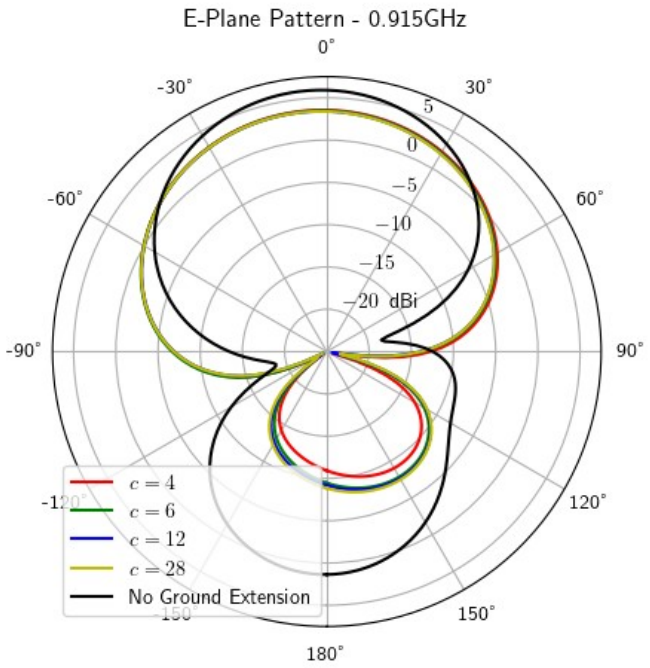

(a)

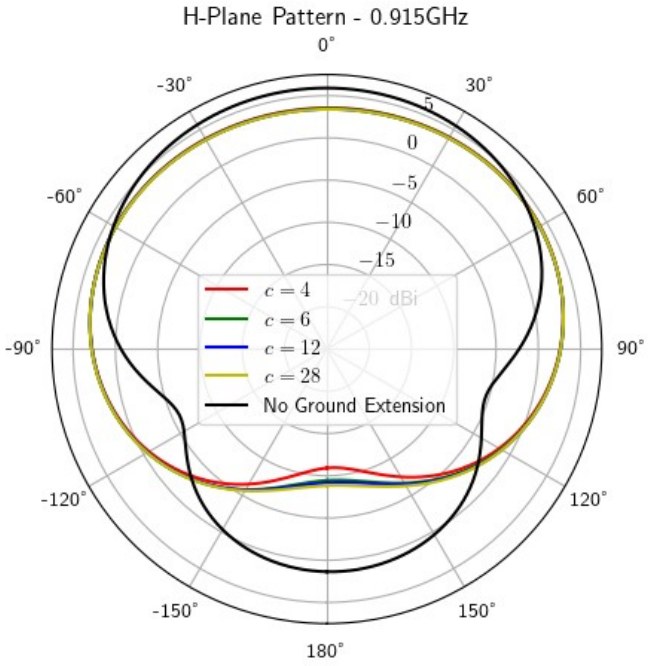

(b)

Fig. 4.6: E-plane (a) and H-plane (b) radiation patterns at 0.915 GHz for a variety of values of the coefficient *c*.

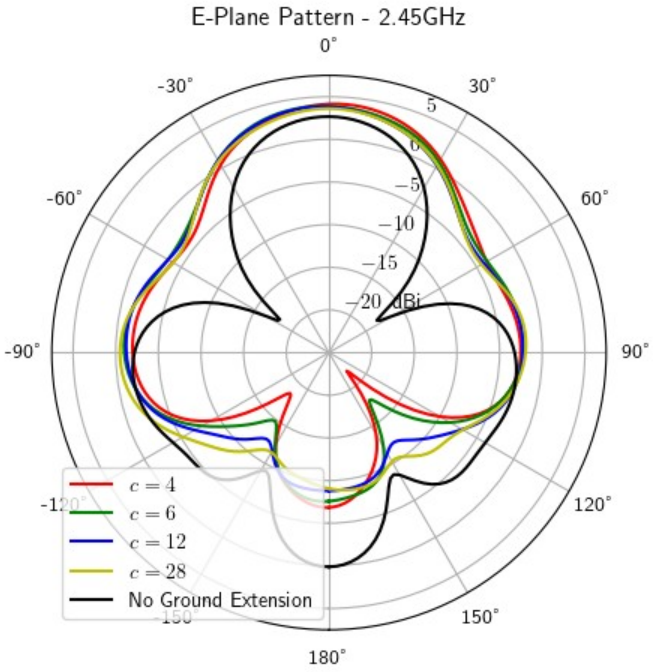

(a)

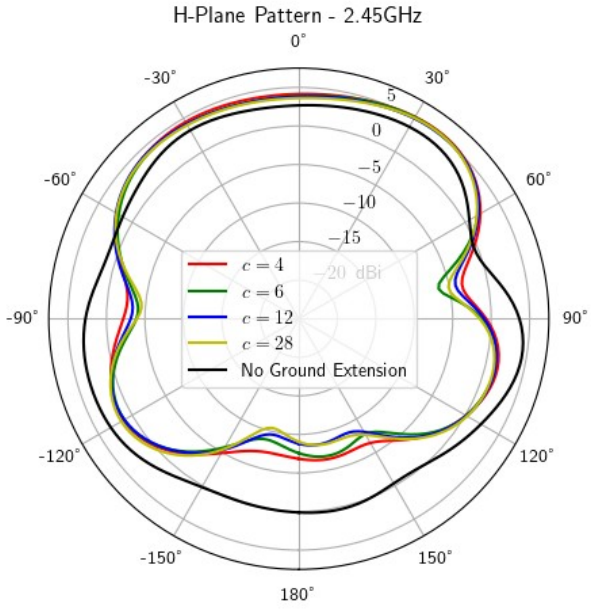

(b)

Fig. 4.7: E-plane (a) and H-plane (b) radiation patterns at 2.45 GHz for a variety of values of the coefficient c.

4.4 Reduced Ground Plane Size

Since compactness is a design goal for this antenna, efforts were taken to reduce the size of the antenna board down from the 150 mm by 150 mm size used for the prototype. While miniaturizing below 120 mm by 120 mm imposed significant difficulties in achieving good radiation in the upper band, the 120 mm by 120 mm design was more tractable and is presented here. The antenna with this reduced ground plane is shown in Fig. 4.8; the main addition to the geometry are the slots present on either side of the ground plane. These slots are approximately 0.25 λ_1 and 0.75 λ_2, where λ_1 and λ_2 are the wavelengths along the microstrip feed line as calculated by AWR TX-LINE [40] for the 0.915 GHz and 2.45 GHz, respectively. From the microwave engineering point of view, the slots are equivalent to short-circuited quarter- and three-quarter wavelength transmission lines, mimicking a high input impedance line that will eventually reduce the unwanted back radiation.

The effect of these short-circuited lines is laid out in Eqs. 4.3 - 4.5. Eq. 4.3 is the general equation for the input impedance Z_{in} of a lossless transmission line with length l and phase constant β connected to a load of impedance Z_L as given by Pozar [41]. Since the choke slots are of electrical length $\beta l = \pi/2$ at the lower band and $\beta l = 3\pi/2$ at the upper band, Z_{in} in these cases is simplified as shown in Eq. 4.4. Finally, since we are considering the short-circuit case we have $Z_L \rightarrow 0$, resulting in Eq. 4.5. This gives us the high input impedance behavior needed to suppress the back lobe.

$$Z_{\text{in}} = Z_0 \frac{Z_L + jZ_0 \tan \beta l}{Z_0 + jZ_L \tan \beta l} \tag{4.3}$$

$$Z_{\text{in}}\Big|_{\beta l = \pi/2, 3\pi/2} = \frac{Z_0^2}{Z_L} \tag{4.4}$$

$$Z_{\text{in}}\Big|_{Z_L \to 0} \to \infty \tag{4.5}$$

The simulated S_{11} performance for this antenna with and without choke slots is presented in Fig. 4.9. This reduced ground plane antenna with slots maintains good impedance matching at the target frequencies with return loss of 31.5 dB at 0.915 GHz and 20.7 dB at 2.45GHz. However, in the upper band it can be seen that the two resonances are separated by a more significant decrease in return loss; at 2.54 GHz, the return loss barely reaches 10 dB, potentially establishing a stricter limit on the usable bandwidth. The addition of slots to this design aided with impedance matching at 2.45 GHz at the expense of the second resonance in the upper band.

The E-plane and H-plane cuts of the antenna pattern are shown in Fig. 4.10 for the 0.915 GHz band. Moving the ground plane closer to the antenna resulted in a suppression of the back lobe and a slight increase in the forward gain from 3.41 dBi for the full-size antenna to 4.15 dBi in the reduced-size case without slots. The front-to-back ratio was also improved from 12.58 dB to 14.76 dB. Adding slots slightly degraded performance in the lower band with 3.78 dBi and front-to-back ratio of 11.95 dB; these are still within acceptable limits.

In Fig. 4.11 we see the effect of the ground plane chokes on the reduced-size design. The peak gain of 4.16 dBi for the slotted antenna is better than that of the antenna without slots at 3.18 dBi and the full-size antenna at 3.81 dBi. The front-to-back ratio is

also improved, giving 13.42 dB for the slotted design compared to 9.24 dB for the antenna without slots and 12.61 dB for the full-size. The addition of the chokes on the ground plane provided approximately 4 dB of improvement to the front-to-back ratio, bringing it to an acceptable value. Fig. 4.11b also shows that the H-plane pattern for the slotted design exhibits much greater symmetry and uniformity in the forward direction, which is desirable. It can be seen from Figs. 4.10 and 4.11 that adding slots improves upper-band radiation performance at the expense of some lower-band radiation performance, allowing us to achieve acceptable operation in both bands.

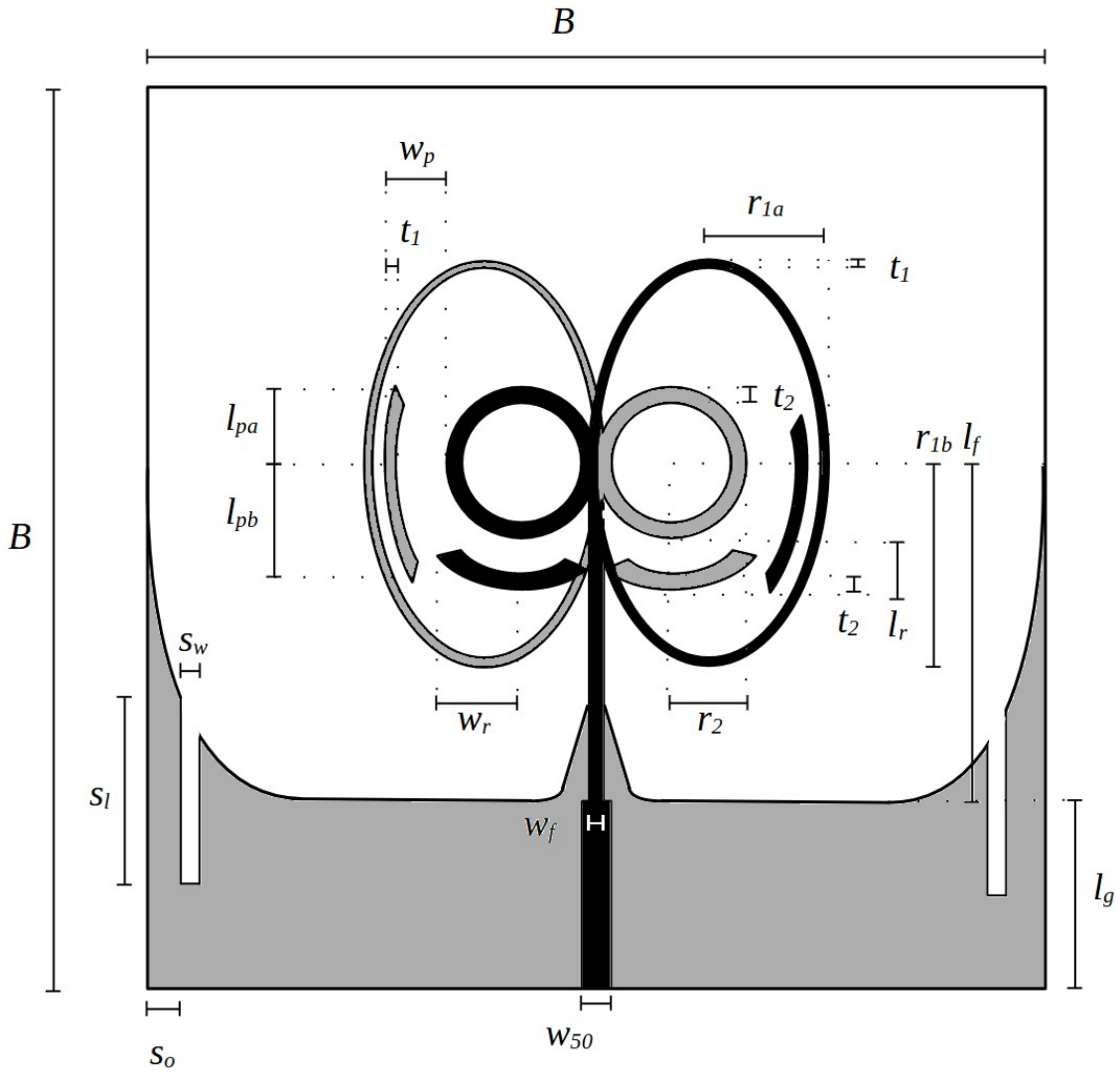

Fig. 4.8: Geometry of an antenna with reduced ground plane size having dimensions r_a = 21.4 mm, $r1b$ = 38.5 mm, r_2 = 9.8 mm, t_1 = 0.2 mm, and t_2 = 0.4 mm. The top layer is shown in black and the bottom layer in gray. The antenna has reflectors behind the upper-band arms; these are circular sections concentric with the upper-band arms with radii $r_2 + l_r$ where l_r = 5 mm. The reflectors are defined only within the outer ellipse and extend outward by w_r = 22.05 mm. There are also parasitics 2.3 mm inside and concentric with the lower-band arms with l_{pa} = 15mm and l_{pb} = 25 mm. The antenna is fed by a 50 Ω microstrip line with w_{50} = 0.93 mm from a wave port excitation source to a feed line with l_f = 52.5 mm and w_f = 0.5 mm. The ground plane extends l_g = 14.5 mm with slots governed by s_w = 2 mm, s_l = 32.5 mm, and s_o = 4 mm. The substrate is Rogers Kappa 438 (εr = 4.38) with a thickness of 0.11 mm, and the board size (B) is 120 mm.

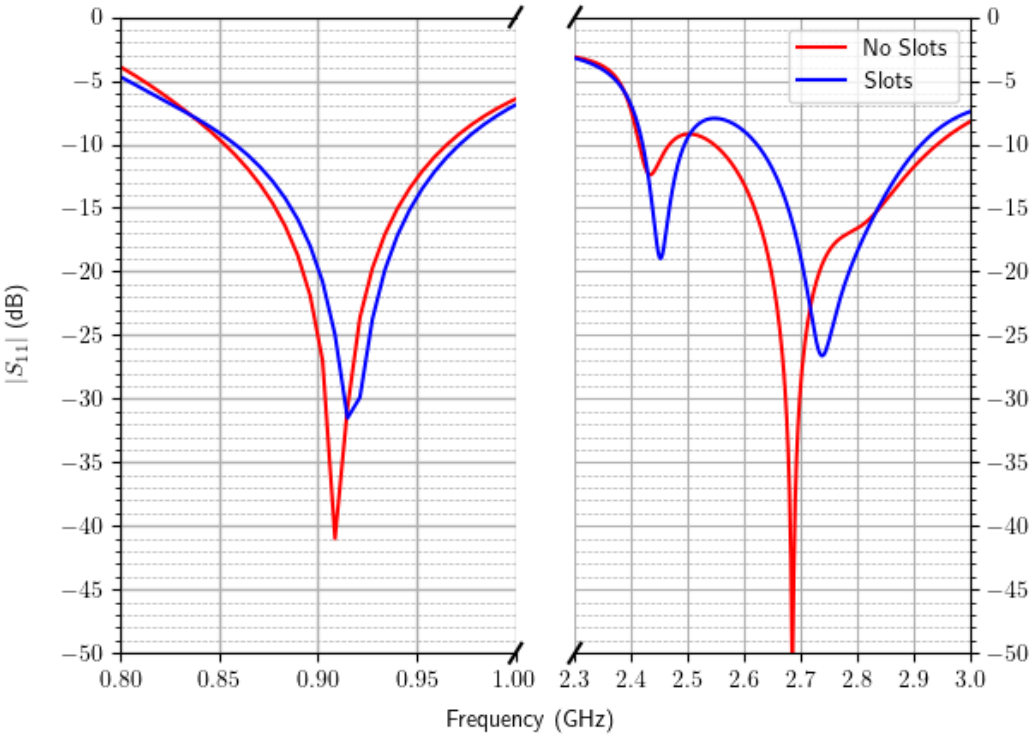

Fig. 4.9: Simulated $|S_{11}|$ versus frequency for both the lower and upper bands for the reduced ground plane antenna shown in Fig. 4.8 with and without slots.

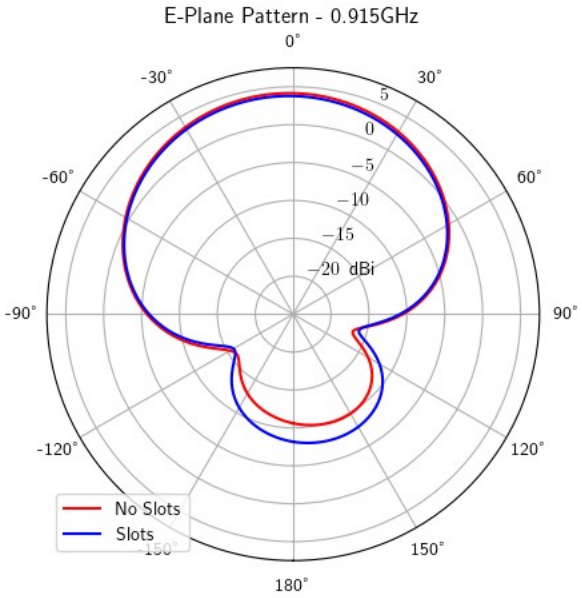

(a)

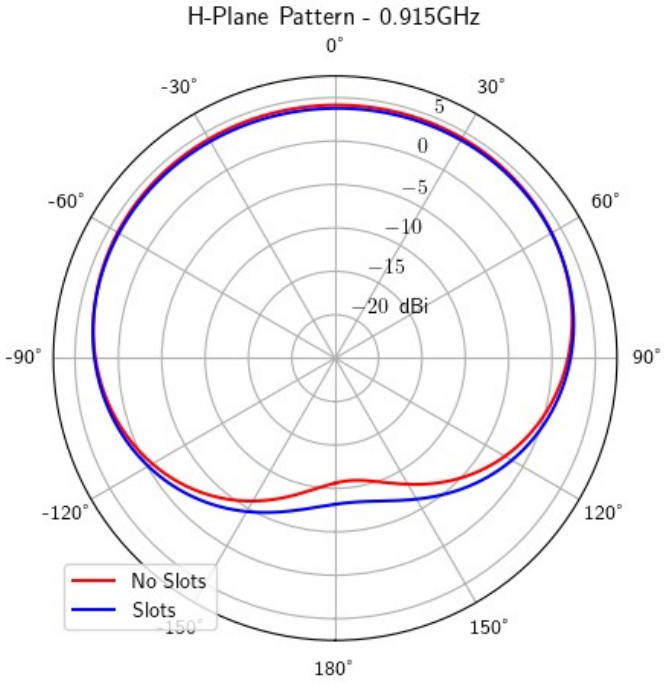

(b)

Fig. 4.10: Simulated E-plane (a) and H-plane (b) radiation patterns at 0.915 GHz for the antenna shown in Fig. 4.8 with and without slots.

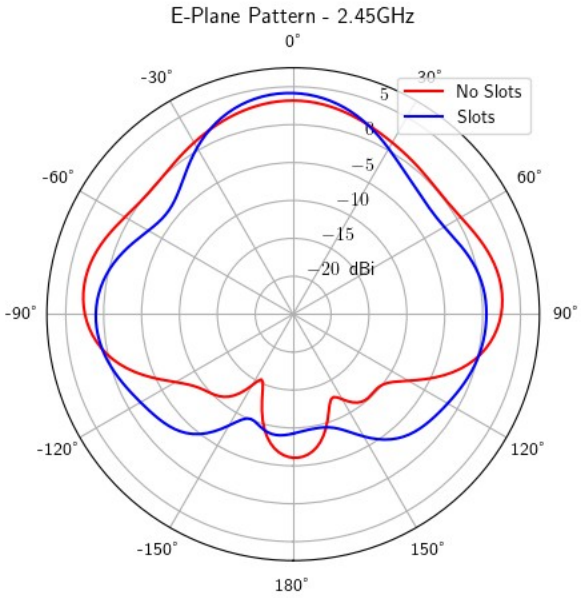

(a)

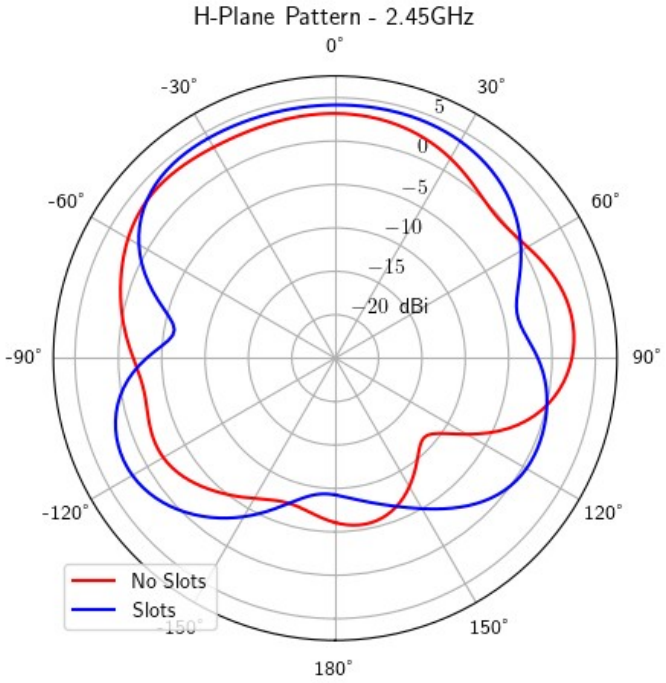

(b)

Fig. 4.11: Simulated E-plane (a) and H-plane (b) radiation patterns at 2.45 GHz or the antenna shown in Fig. 4.8 with and without slots.

4.5 Summary

A few variations of the dual-band elliptical antenna are presented in Chapter 4. First, a parametric sweep of the semi-major axis gave some insight into the effects of the eccentricity of the lower-band arm. The resonant frequency was found to have an inverse relationship to the elliptical circumference, and the higher eccentricity was seen to improve the front-to-back ratio in the upper band. A sweep of a parameter controlling the shape of the exponential ground showed that antenna performance is insensitive to this shape. Finally, a reduction in the size of the ground plane was presented; adding ground chokes was found to mitigate the negative effects of this reduction on the upper-band back lobe suppression.

CHAPTER 5

Measurement Results

5.1 Introduction

For validation purposes, the design in Fig. 3.20 with both reflectors and parasitics was then sent for fabrication by PCB manufacturer Advanced Circuitry International in Atlanta. The substrate used was 0.11 mm thick Rogers Kappa 438 material. Upon receipt of the antenna, an edge-mount SMA connector was soldered to the board. This prototype antenna was then measured with a network analyzer and the spherical near-field anechoic chamber of the University of Alabama in Huntsville (UAH); the results are presented here in comparison to simulation.

5.2 Measured Data

Pictures of the top and bottom of the manufactured antenna prototype are shown in Figs. 5.1 and 5.2, respectively. The manufactured antenna is displayed in UAH's anechoic chamber in Fig. 5.3.

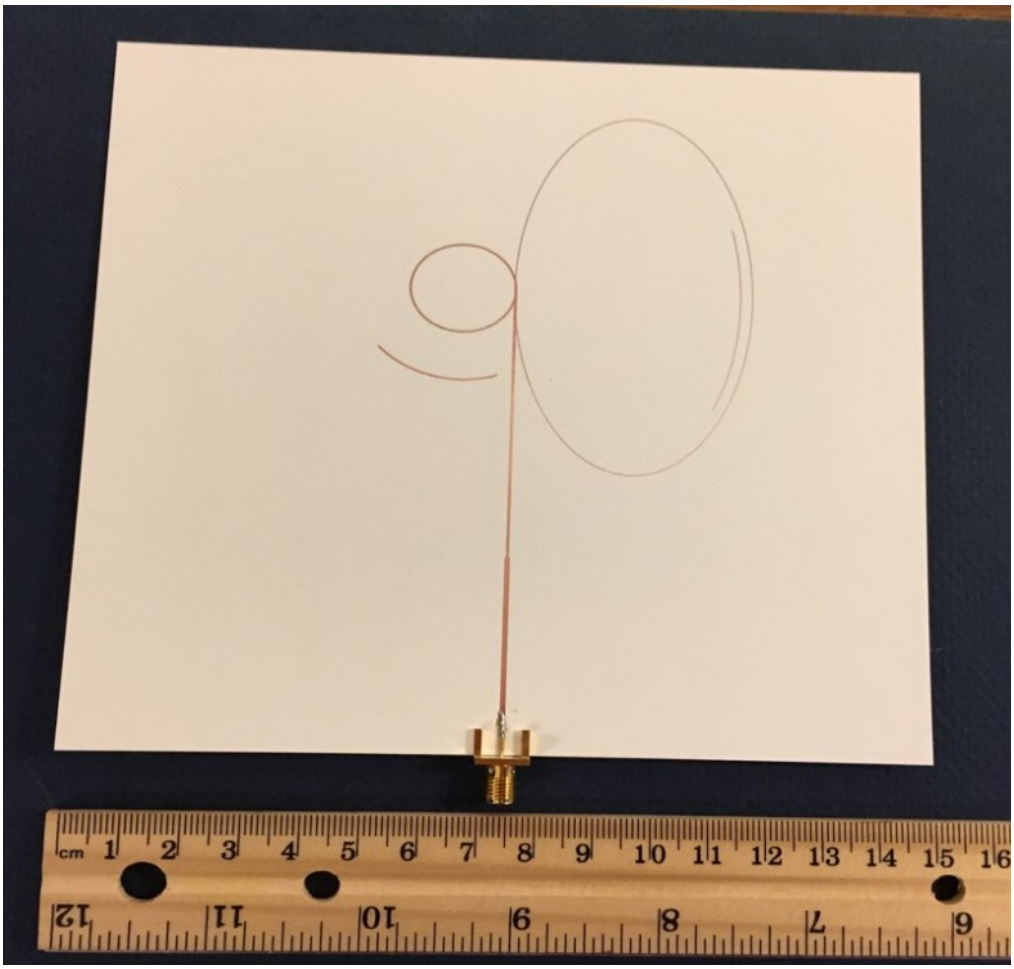

Fig. 5.1: Top side of the manufactured antenna prototype.

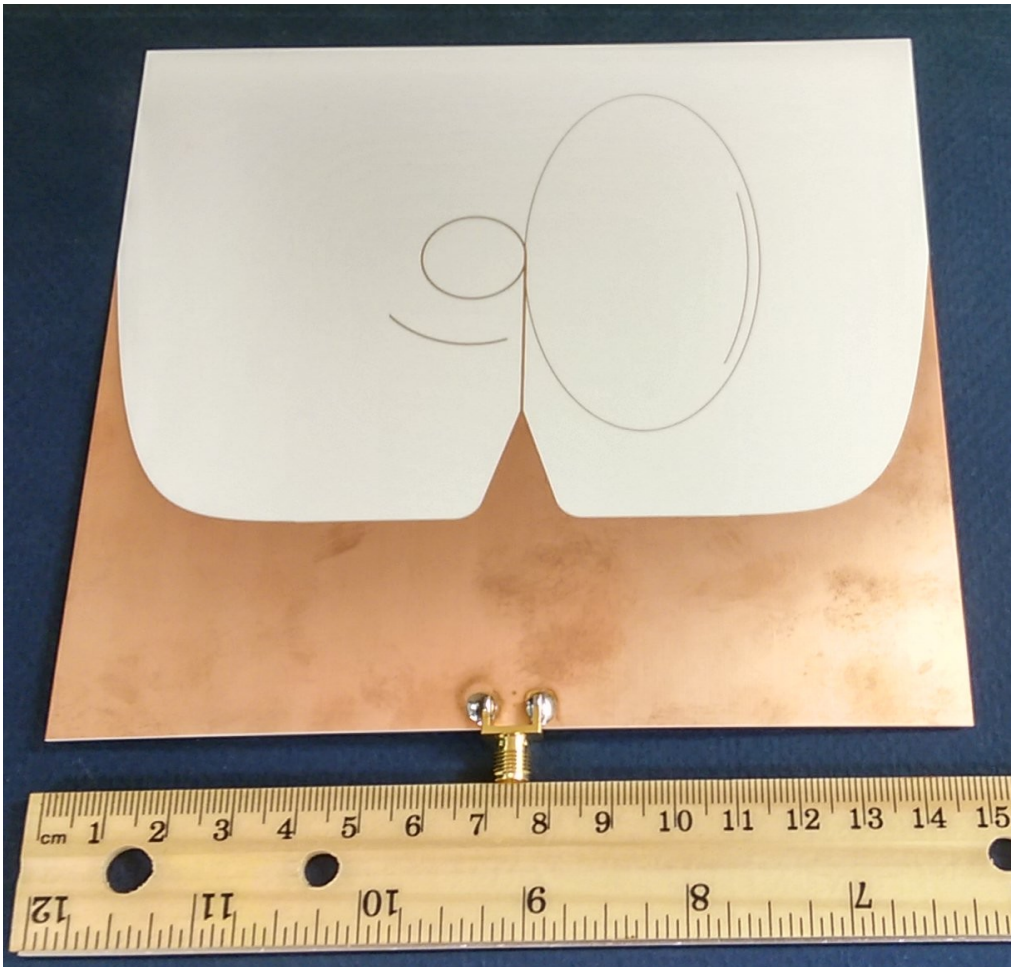

Fig. 5.2: Bottom side of the manufactured antenna prototype.

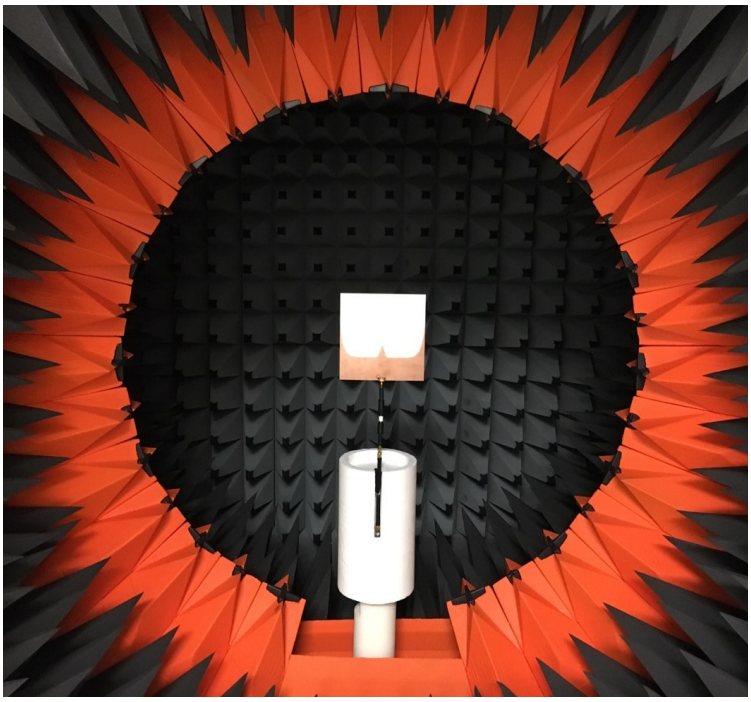

(a)

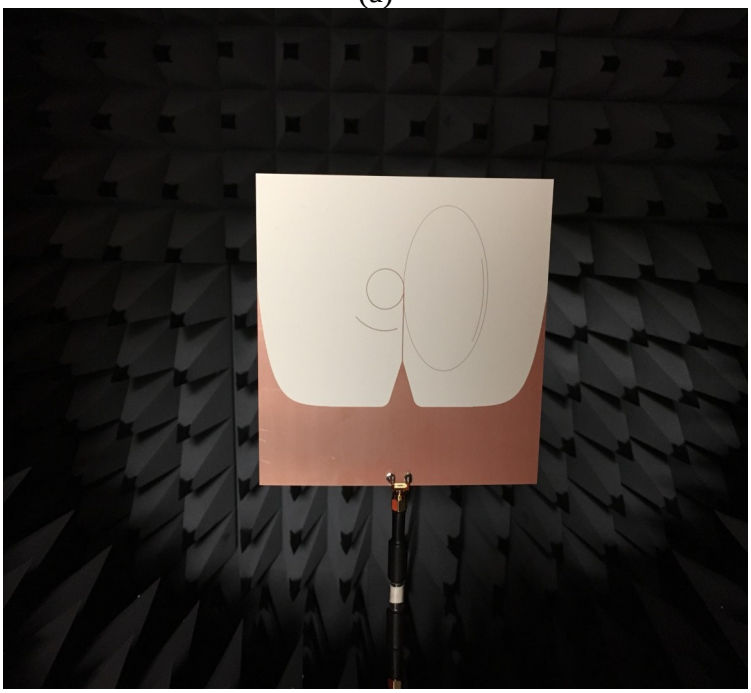

(b)

Fig. 5.3: The manufactured antenna prototype in UAH's spherical near-field anechoic chamber (a) and a closer shot of the bottom of the antenna in the chamber (b).

The upper-band portion of Fig. 5.4 shows that there are two different resonant frequencies which contribute to the wideband nature of the upper band. The first of these resonances is close to the design frequency; in simulation, it is 2.44 GHz and in measurement it is 2.46 GHz. The second of these resonances, 2.66 GHz in simulation and 2.71 GHz in the measured data, is closer to three times the lower-band design frequency.

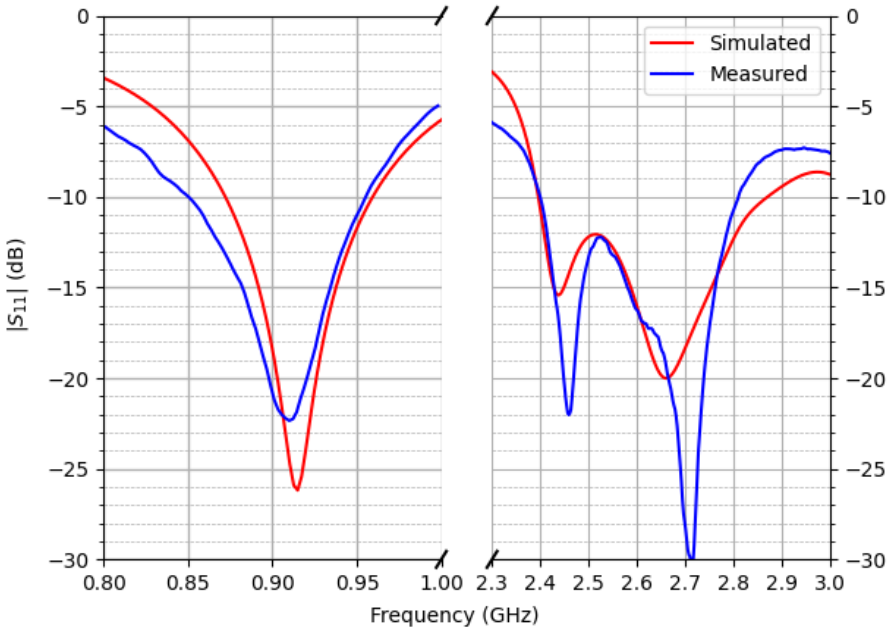

Fig. 5.4: Simulated and measured $|S_{11}|$ versus frequency for both the lower and upper bands.

The antenna radiation patterns were also measured in UAH's near-field anechoic chamber at both 0.915 GHz and 2.45 GHz. The lower band patterns for the E-plane and H-plane cuts are compared to the simulated results in Fig. 5.5, while the upper band patterns are shown in Fig. 5.6. Fig. 5.5 shows a more pronounced back lobe for the measured antenna in the lower band; this is in part attributed to the reflections caused by

the connecting cable in the anechoic chamber.

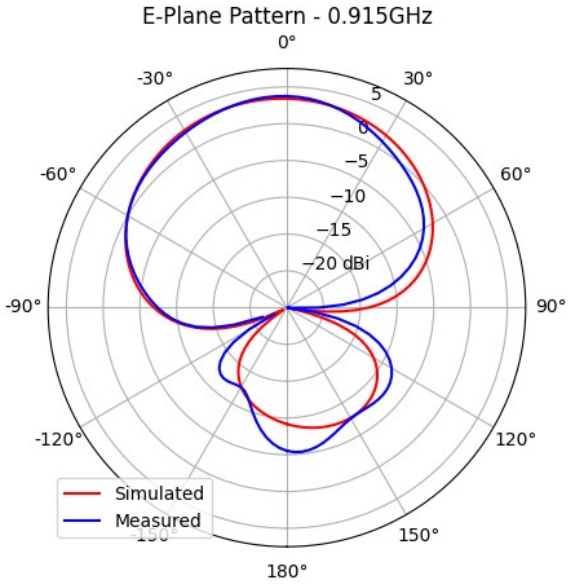

(a)

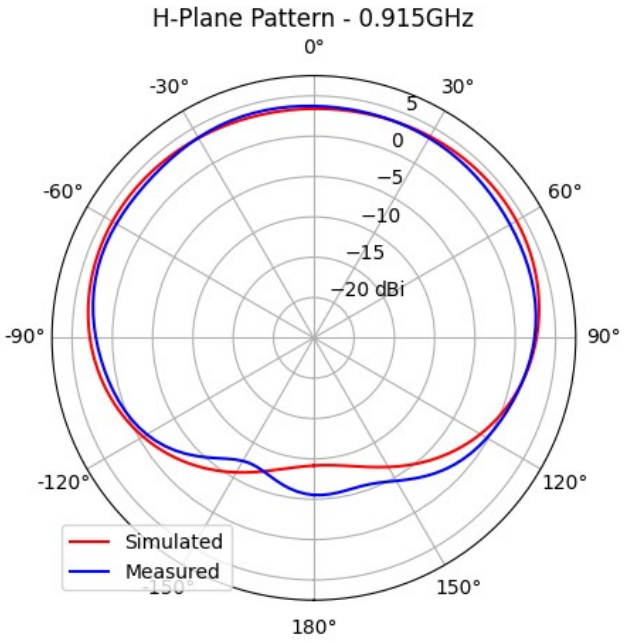

(b)

Fig. 5.5: Simulated and measured E-plane (a) and H-plane (b) radiation patterns at 0.915 GHz.

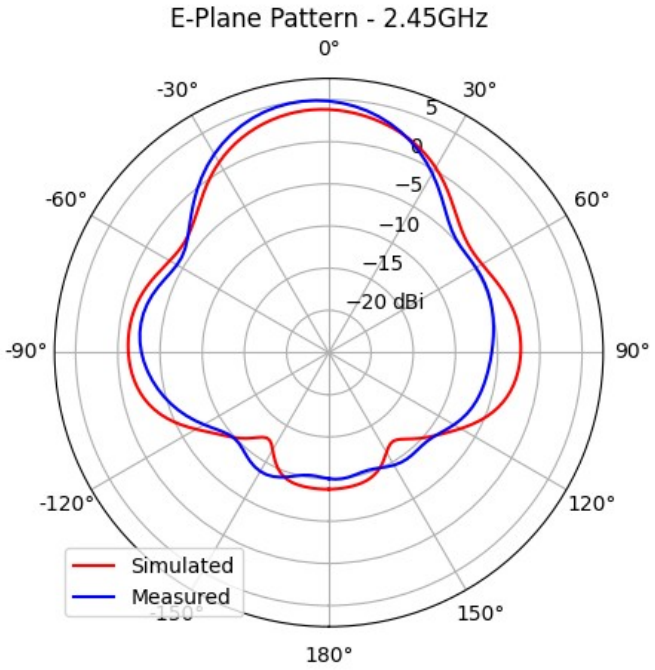

(a)

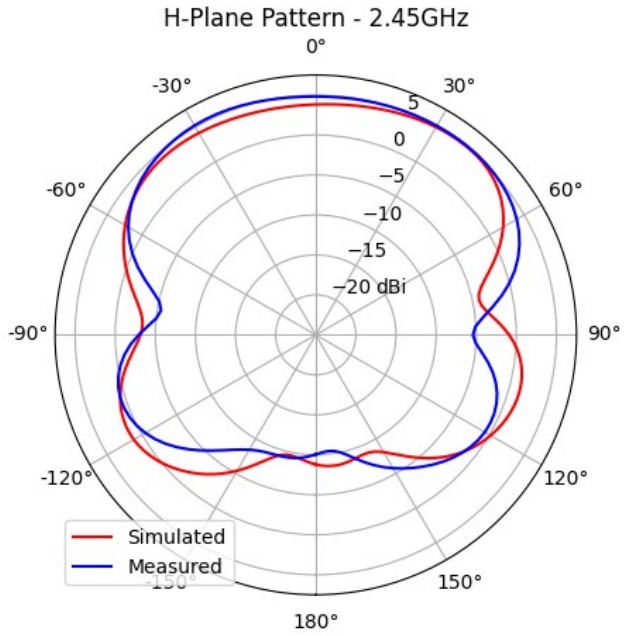

(b)

Fig. 5.6: Simulated and measured E-plane (a) and H-plane (b) radiation patterns at 2.45 GHz.

Table 5.1: Quantities of interest compared between the simulated design and the prototype measurements at both the lower (0.915 GHz) and upper (2.45 GHz) bands.

	Simulated Result	Measured Result
Peak Gain at 0.915 GHz	3.41 dBi	3.75 dBi
Front-to-Back Ratio at 0.915 GHz	12.58 dB	9.28 dB
Return Loss at 0.915 GHz	26.19 dB	21.87 dB
Lower-band 10 dB Bandwidth	85 MHz	103 MHz
Peak Gain at 2.45 GHz	3.82 dBi	4.81 dBi
Front-to-Back Ratio at 2.45 GHz	12.61 dB	14.86 dB
Return Loss at 2.45 GHz	14.86 dB	20.47 dB
Upper-band 10 dB Bandwidth	472 MHz	407 MHz

Table 5.1 shows that most of the results are approximately what the simulation predicts. The 10 dB impedance bandwidths, though different from the simulation, are still acceptable. Similarly, the measured front-to-back ratio at 0.915 GHz is close to the desired 10 dB, and some degradation is to be expected due to the mounting setup in the anechoic chamber. Finally, the measured peak gain at 2.45 GHz is nearly 1 dB greater than its simulated value, seemingly due to gain errors of the antenna test range.

5.3 Summary

The dual-band antenna design with additional reflective and parasitic elements shown in Fig. 3.20 was fabricated on a PCB. An edge-mount SMA connector was soldered to the board and measurements were carried out. The measured results for impedance matching agree well with the simulated results, with the resonant frequencies in each band being close in measurement and simulation. The antenna patterns are also

good in agreement, especially at 2.45 GHz. The back lobe at 0.915 GHz is more pronounced for the measured antenna. The forward gain was measured at 3.75 dBi at 0.915 GHz and 4.81 dBi at 2.45 GHz.

CHAPTER 6

Conclusions and Future Work

A novel dual-band elliptical antenna design was presented in this thesis. First, the literature regarding low-profile antennas, elliptical antennas, outline antennas, and inset dual-band designs was summarized. The dual-band elliptical antenna was then constructed by iterating on a single-band, filled dipole antenna design. First the metallization was removed, resulting in a much more compact antenna with narrower bandwidth. Then, additional upper-band elements were set within the lower-band arms to create an inset antenna. The upper-band performance was poor due to mutual coupling, so the upper-band element was reflected across the feed line to achieve phase reversal, creating the opposed antenna design. Finally, additional improvements were added in the way of an extended, exponentially tapered ground plane, reflectors behind the upper-band elements, and parasitics within the lower-band elements. At both 0.915 GHz and 2.45 GHz, this proposed antenna achieved greater than 14 dB return loss, 3.4 dBi peak gain, and 12 dB front-to-back ratio.

Several simulation scenarios were derived from this proposed design. The first varied the semi-major axis of the outer ellipse while keeping the semi-minor axis constant to observe a variety of eccentricities. It was concluded that the resonant frequency has a roughly inverse dependence on the elliptical circumference and that

higher eccentricities had more desirable upper-band radiation performance. The shape of the exponential ground taper was also varied; while performance suffered when this extended portion of the ground too closely approached the lower-band antenna arms, after sufficient separation was reached the antenna performance was insensitive to this shape. Finally, a reduction in the size of the ground plane was undertaken. The board size was reduced from 150 mm by 150 mm to 120 mm by 120 mm, causing a slight degradation in radiation characteristics at the upper band. The addition of chokes at the edges of the ground plane recovered that lost upper-band performance.

A prototype of the dual-band elliptical design on the full-sized board was manufactured and measured, and the measurements were found to be in good agreement with their simulated counterparts. Greater than 20 dB return loss, 3.75 dBi peak gain, and close to 10 dB return loss were all achieved with this prototype at both 0.915 GHz and 2.45 GHz. This successfully validates the simulated design and shows the value of this low-profile, lightweight antenna design in the areas of passive energy harvesting.

FUTURE WORK:

- Investigate antenna miniaturization techniques to increase the compactness of the antenna such as meandering the lower-band arm or forming fractal arms.
- Use the proposed antenna as elements to populate a phased array antenna for increased power reception.
- Integrate dual-band impedance matching and rectification circuits on the same PCB to complete a “rectenna” design.

- Consider the effects of placing additional antenna elements within the structure to extend the multi-band properties of this design.

Bibliography

[1] W. C. Brown, "The History of Power Transmission by Radio Waves," *IEEE Transactions on Microwave Theory and Techniques*, vol. 32, no. 9, pp. 1230-1242, Sep. 1984.

[2] J. O. McSpadden, F. E. Little, M. B. Duke and A. Ignatiev, "An in-space wireless energy transmission experiment*," IECEC 96. Proceedings of the 31st Intersociety Energy Conversion Engineering Conference*, Washington, DC, USA, 1996.

[3] W. Wilkinson, "A class of printed circuit antennas*," 1974 Antennas and Propagation Society International Symposium*, Atlanta, GA, USA, 1974.

[4] M. Arrawatia, M. S. Baghini and G. Kumar, "Broadband Bent Triangular Omnidirectional Antenna for RF Energy Harvesting*," IEEE Antennas and Wireless Propagation Letters*, vol. 15, pp. 36-39, Apr. 2015.

[5] B. G. Duffley, G. A. Morin, M. Mikavica and Y. M. M. Antar, "A wide-band printed double-sided dipole array," *IEEE Transactions on Antennas and Propagation*, vol. 52, no. 2, pp. 628-631, Feb. 2004.

[6] Z. Tu, G. Zhang, D. Zhou and F. Xing, "A wideband elliptic printed dipole antenna array*," 2011 4th IEEE International Symposium on Microwave, Antenna, Propagation and EMC Technologies for Wireless Communications*, Beijing, China, 2011.

[7] J. A. Hagerty, F. B. Helmbrecht, W. H. McCalpin, R. Zane and Z. B. Popovic, "Recycling ambient microwave energy with broad-band rectenna arrays," *IEEE Transactions on Microwave Theory and Techniques*, vol. 52, no. 3, pp. 1014-1024, Mar. 2004.

[8] Warren L. Stutzman & Gary A. Thiele, "Antenna Theory and Design, 3rd Ed.", Hoboken, NJ, USA: J. Wiley, pp. 235-266, 2012.

[9] K. Bahadori and Y. Rahmat-Samii, "A Miniaturized Elliptic-Card UWB Antenna With WLAN Band Rejection for Wireless Communications," *IEEE Transactions on Antennas and Propagation*, vol. 55, no. 11, pp. 3326-3332, Nov. 2007.

[10] K. P. Ray and Y. Ranga, "Ultrawideband Printed Elliptical Monopole Antennas," *IEEE Transactions on Antennas and Propagation*, vol. 55, no. 4, pp. 1189-1192, Apr. 2007.

[11] N. P. Agrawall, G. Kumar and K. P. Ray, "Wide-band planar monopole antennas,"

IEEE Transactions on Antennas and Propagation, vol. 46, no. 2, pp. 294-295, Feb. 1998.

[12] Kiminami, Hirata and Shiozawa, "Double-sided printed bow-tie antenna for UWB communications," *IEEE Antennas and Wireless Propagation Letters*, vol. 3, pp. 152-153, 2004.

[13] T. Karacolak and E. Topsakal, "A Double-Sided Rounded Bow-Tie Antenna (DSRBA) for UWB Communication," *IEEE Antennas and Wireless Propagation Letters*, vol. 5, no. , pp. 446-449, Oct. 2006.

[14] M. Pergol and W. Zieniutycz, "New planar dipole radiator for UWB application," *MIKON 2008 - 17th International Conference on Microwaves, Radar and Wireless Communications*, Wroclaw, Poland, 2008.

[15] H. G. Schantz, "Planar elliptical element ultra-wideband dipole antennas," *IEEE Antennas and Propagation Society International Symposium*, San Antonio, TX, USA, 2002.

[16] J. Powell and A. Chandrakasan, "Differential and single ended elliptical antennas for 3.1-10.6 GHz ultra wideband communication," *IEEE Antennas and Propagation Society Symposium*, Monterey, CA, USA, 2004.

[17] Chun-Chi Lee, Chia-Wei Wang, R. Y. Yen and Hsin-Sheng Huang, "Broadband printed-circuit elliptical dipole antenna covering 750 MHz–6.0 GHz," *2008 International Conference on Microwave and Millimeter Wave Technology*, Nanjing, China, 2008.

[18] L. Sorokosz and W. Zieniutycz, "On the Approximation of the UWB Dipole Elliptical Arms With Stepped-Edge Polygon," *IEEE Antennas and Wireless Propagation Letters*, vol. 11, pp. 636-639, Jun. 2012.

[19] A. C. Durgun, C. A. Balanis, C. R. Birtcher and D. R. Allee, "Design, Simulation, Fabrication and Testing of Flexible Bow-Tie Antennas," *IEEE Transactions on Antennas and Propagation*, vol. 59, no. 12, pp. 4425-4435, Dec. 2011.

[20] H. Nakano, S. Hattori, H. Mimaki, and J. Yamauchi, "A Card-Type Wide Band Antenna," *International Symposium on Antennas and Propagation*, Seoul, Korea, 2005.

[21] N. C. Azenui and H. Y. D. Yang, "A Printed Crescent Patch Antenna for Ultrawideband Applications," *IEEE Antennas and Wireless Propagation Letters*, vol. 6, pp. 113-116, Apr. 2007.

[22] A. M. Abbosh and M. E. Bialkowski, "Design of Ultrawideband Planar Monopole Antennas of Circular and Elliptical Shape," *IEEE Transactions on Antennas and Propagation*, vol. 56, no. 1, pp. 17-23, Jan. 2008.

[23] D. H. Werner, "Exact Expressions for the Far-Zone Electromagnetic Fields Radiated by Thin Elliptical Loop Antennas of Arbitrary Size," *IEEE Transactions on Antennas and Propagation*, vol. 66, no. 12, pp. 6844-6850, Dec. 2018.

[24] H. Nazli, E. Bicak, B. Turetken and M. Sezgin, "An Improved Design of Planar Elliptical Dipole Antenna for UWB Applications," *IEEE Antennas and Wireless Propagation Letters*, vol. 9, pp. 264-267, . 2010.

[25] E. N. Tziris, P. I. Lazaridis, Z. D. Zaharis, J. P. Cosmas, K. K. Mistry and I. A. Glover, "Optimized Planar Elliptical Dipole Antenna for UWB EMC Applications," *IEEE Transactions on Electromagnetic Compatibility*, vol. 61, no. 4, pp. 1377-1384, Aug. 2019.

[26] V. De Noia, A. Alves, M. Diaz and R. Barroso, "Input impedance behavior of a planar elliptical ring dipole antenna," *Proceedings of the 2012 IEEE International Symposium on Antennas and Propagation*, Chicago, IL, USA, 2012.

[27] S. Maci, G. Biffi Gentili, P. Piazzesi and C. Salvador, "Dual-band slot-loaded patch antenna," *IEE Proceedings - Microwaves, Antennas and Propagation*, vol. 142, no. 3, pp. 225-232, Jun. 1995.

[28] Sung Min Kim and Woon Geun Yang, "Design and implementation of dual wideband sleeve dipole type antenna for the reception of S-DMB and 2.4/5GHZ WLAN signals," *2006 IEEE Antennas and Propagation Society International Symposium*, Albuquerque, NM, USA, 2006.

[29] Yen-Liang Kuo and Kin-Lu Wong, "Printed double-T monopole antenna for 2.4/5.2 GHz dual-band WLAN operations," *IEEE Transactions on Antennas and Propagation*, vol. 51, no. 9, pp. 2187-2192, Sep. 2003.

[30] R. K. Joshi and A. R. Harish, "A Modified Bow-Tie Antenna for Dual Band Applications," *IEEE Antennas and Wireless Propagation Letters*, vol. 6, pp. 468-471, Oct. 2007.

[31] P. Wu, Z. Kuai and X. Zhu, "Multiband Antennas Comprising Multiple Frame-Printed Dipoles," *IEEE Transactions on Antennas and Propagation*, vol. 57, no. 10, pp. 3313-3316, Oct. 2009.

[32] C. T. P. Song, P. S. Hall and H. Ghafouri-Shiraz, "Multiband multiple ring monopole antennas," *IEEE Transactions on Antennas and Propagation*, vol. 51, no. 4, pp. 722-729, Apr. 2003.

[33] C. Kumar and D. Guha, "Mitigating Backside Radiation Issues of Defected Ground Structure Integrated Microstrip Patches," *IEEE Antennas and Wireless Propagation*

Letters, vol. 19, no. 12, pp. 2502-2506, Dec. 2020.

[34] M. A. Antoniades and G. V. Eleftheriades, "A Compact Multiband Monopole Antenna With a Defected Ground Plane," *IEEE Antennas and Wireless Propagation Letters*, vol. 7, pp. 652-655, Oct. 2008.

[35] A. A. Kishk and L. Shafai, "Optimization of microstrip feed geometry for prime focus reflector antennas," *IEEE Transactions on Antennas and Propagation*, vol. 37, no. 4, pp. 445-451, Apr. 1989.

[36] W. Lim, H. Jang and J. Yu, "New method for back lobe suppression of microstrip patch antenna for GPS," *The 40th European Microwave Conference*, Paris, France, 2010.

[37] Rogers Corporation, "Kappa 438 Laminates," *Kappa 438 Datasheet*, [Revised 2019].

[38] ANSYS, Inc., Canonsburg, PA, USA, "Ansys HFSS for Antenna Simulation," 2020.

[39] J. C. Marquardt, M. Pour, C. Hill, and I. Small, "A Novel Dual-Band Outlined Elliptical Dipole Antenna for Passive Energy Harvesting," accepted in the *2021 IEEE Int. Symp. Antennas Propag. & USNC/URSI National Radio Science Meeting*, Marina Bay Sands, Singapore, Dec. 4-10, 2021.

[40] Cadence Design Systems, Inc., San Jose, CA, USA, "TX-LINE Transmission-Line Calculator," 2003.

[41] David M. Pozar, "Microwave Engineering, 4th Ed.", Hoboken, NJ, USA: J. Wiley, pp. 59, 2012.